

A CCD Search for Variable Stars in the Open Cluster NGC 6611

G. Michalska,^{1,2*} Z. Kołaczkowski^{1,2,†}, R. Leiton,^{3,4} O. Szewczyk², K. Kinemuchi², V. M. Kalari,⁵

¹Uniwersytet Wrocławski, Instytut Astronomiczny, Kopernika 11, 51-622 Wrocław, Poland

²Universidad de Concepción, Departamento de Astronomía, Chile

³Las Campanas Observatory, Carnegie Institution for Science, Colina el Pino, Casilla 601 La Serena, Chile

⁴CePIA, Departamento de Astronomía, Universidad de Concepción, Casilla 160-C, Concepción, Chile

⁵Gemini Observatory, Southern Operations Center, c/o AURA, Casilla 603, La Serena, Chile

Accepted XXX. Received YYY; in original form ZZZ

ABSTRACT

We present the results of the $UBVI_C$ variability survey in the young open cluster NGC 6611 based on observations obtained during 34 nights spanning one year. In total, we found 95 variable stars. Most of these stars are classified as periodic and irregular pre-main sequence (PMS) stars. The analysis of the JHK_S 2MASS photometry and four-colour IRAC photometry revealed 165 Class II young stellar sources, 20 of which are irregular variables and one is an eclipsing binary. These classifications, complemented by JHK UKIDSS photometry and $riH\alpha$ VPHAS photometry, were used to identify 24 candidates for classical T Tauri stars and 30 weak-lined T Tauri stars. In addition to the PMS variables, we discovered eight δ Scuti candidates. None of these were previously known. Furthermore, we detected 17 eclipsing binaries where two were previously known. Based on the proper motions provided by the Gaia EDR3 catalogue, we calculated the cluster membership probabilities for 91 variable stars. For 61 variables, a probability higher than 80% was determined, which makes them cluster members. Only 25 variables with a probability less than 20% were regarded to be non-members.

Key words: open clusters and associations: individual: NGC 6611 – stars: pre-main sequence – stars: variables: T Tauri, Herbig Ae/Be, δ Scuti stars, eclipsing binaries.

1 INTRODUCTION

Many stars in very young open clusters are in the pre-main sequence (PMS) stage of evolution. Depending on their mass, PMS stars are divided into two groups: low mass ($< 2 M_\odot$) T Tauri stars (TTSs) with an outer convective zone and intermediate mass ($\sim 2\text{--}10 M_\odot$) Herbig Ae/Be stars (HAeBe). Both groups of PMS stars shows different types of photometric variability.

As a class of variable stars, TTSs stars were first defined by Joy (1945), who selected a group of F5–G5 stars with fast irregular light variations. These variations are indicated by emission lines resembling the solar chromosphere and/or are associated with a dark or bright nebulosity. Nowadays, such stars are characterized by a strong emission in the H and K Ca II and $H\alpha$ lines (with equivalent widths $EW_{H\alpha} > 10 \text{ \AA}$) and are known as classical TTSs (CTTSs). CTTSs are surrounded by a thick disk detected by infrared excess (Kenyon & Hartmann 1987).

The magnetic field generated by a solar-type dynamo plays an important role in the variability of CTTSs. A strong magnetic field interacts with the inner disk, truncates it at a few

stellar radii, and channels the disk matter onto the stellar surface. The infalling gas produces hot spots and shocks. Dissipated X-ray and EUV radiation interact with the surrounding gas and cause emission at longer wavelengths, which gives the UV and optical continuum excesses. This process, known as magnetospheric accretion, has been modelled for many years (see Koenigl 1991; Shu et al. 1994; Muzerolle et al. 1998; Bouvier et al. 2007; Romanova et al. 2012, and references therein). Unsteady accretion from the circumstellar disk causes irregular light variation of CTTSs with amplitudes up to 2.6 mag in V (Herbst et al. 1994). Non-periodic variability of PMS stars may be caused also by stellar flares, which are characterised by a fast rise and an exponential decay of the light lasting few minutes or hours (Hawley et al. 2014; Kóspál et al. 2018). Additionally, the light curve of CTTSs can be modulated by rotating hot and cool spots. The periodic changes in the light curves also may be due to circumstellar matter surrounding CTTS.

Other TTSs characterized by a weak emission in the $H\alpha$ line (with $EW_{H\alpha} < 10 \text{ \AA}$) are called naked T Tauri stars (Walter 1986) or weak line TTSs (WTTSs; Bertout 1989). They were first detected in X-ray (Walter & Kuhi 1981; Feigelson & Decampli 1981). For many years, these stars were thought to be more evolved than CTTSs (Walter et al. 1988). Some authors (e.g. Petrov 2003) postulated that the existence of an

* E-mail: michalska@astro.uni.wroc.pl

† Deceased

accretion disk depends on initial conditions at the star formation phase. Bertout et al. (2007) analysed the mass and age distribution of TTSSs in the Taurus-Auriga T association and inferred that younger CTTSSs evolve into WTTSSs when their disks are fully accreted by stars. Galli et al. (2015) came to the same conclusion after analysing TTSSs in the Lupus association. In general, WTTSSs do not show the evidence of accretion. The small infrared excesses seen in some WTTSSs come from the cold passive disk. The light variations of WTTSSs are attributed to rotational modulation of cool spots with typical periods of 0.5–18 d and amplitudes less than 0.8 mag in V (Herbst et al. 1994).

The more massive counterparts of TTSSs, HAeBe stars, were first defined by Herbig (1960). These B, A or F-type stars with emission lines are often associated with nebulosity. They show an infrared excess due to circumstellar material (gas and dust). Many HAeBe stars show photometric variability related to accretion processes and dust clumps in the surrounding material. The et al. (1994) found that HAeBe stars of spectral type earlier than A0 show small light variations ($\Delta V \leq 0.2$ mag), while those of later spectral types show larger variability ($0.65 \leq \Delta V \leq 3.0$ mag). This may be related to the different properties of Herbig Ae and Herbig Be stars. Many studies (e.g. Vink et al. 2002; Mendigutía et al. 2011; Ababakr et al. 2017) have shown that Herbig Ae stars exhibit accretion features similar to those seen in CTTSSs. These findings have been interpreted as evidence that magnetically controlled accretion also occurs in Herbig Ae stars. In more massive Herbig Be stars, material from the disk is accreted directly onto the star through a so-called boundary layer (see Mendigutía 2020, and references therein). Some Herbig Ae stars and early type TTSSs show irregular, deep (1–3 mag in V) Algol-like drops in brightness. This group of stars is called UX Orionis stars (UXors), after the prototype (Herbst et al. 1994).

Other interesting types of PMS variable types are eruptive FU Orionis (FUors; Herbig 1977) and EX Lupi (EXors; Herbig 1989) stars. These objects show intermittent variability due to an unsteady rate of mass accretion. In the case of FUors, a change of brightness of ~ 3 –6 mag lasts several months, or even years, while EXors repeatedly increase their brightness by ~ 1 –4 mag, and return to their original brightness after several weeks or months.

In this paper, we present the results of a variability survey in the young open cluster NGC 6611. It is one of the youngest open clusters known in the Galaxy with estimated age of less than 3 Myr (e.g. Guarcello et al. 2007). The distance to the NGC 6611 was estimated in the relatively wide range between 1.6 kpc (Kamp 1974) and 2.14 kpc (Kumar et al. 2004). The difficulty in determining the distance accurately is related to the variable and anomalous reddening towards this cluster (Hillenbrand et al. 1993; Guarcello et al. 2007). The ratio of total extinction (A_V) to reddening ($E(B - V)$) was estimated between 3.27 (Guarcello et al. 2007) and 4.37 (Shultz et al. 2021). Recently, using the data of Gaia DR2, Kuhn et al. (2019) calculated the mean cluster parallax of 0.57 ± 0.04 mas, corresponding to a distance of 1740_{-120}^{+130} pc. The newest distance determination of 1706 ± 7 pc, calculated from the Gaia EDR3 data, was published by Stoop et al. (2022). The authors reported of two stellar populations in NGC 6611 – the younger population has an age of 1.3 Myr

and a $A_V = 3.5$ mag, while the older has an age 7.5 Myr and $A_V = 2.0$ mag.

A dozen O-type and 50 early B-type main-sequence stars have been identified among the brightest members. Recent studies have revealed several Be and Ae stars, some of which are Herbig Ae/Be stars (Herbig & Dahm 2001; Martayan et al. 2007). A large fraction of the bright stars in NGC 6611 are known visual and spectroscopic binaries (Duchêne et al. 2001; Evans et al. 2005). The cluster contains a significant population of intermediate and low-mass PMS stars (Hillenbrand et al. 1993; Massey et al. 1995; Oliveira et al. 2005), which is typical for such a young and massive region. Moreover, it is associated with the famous H II and star-forming region, the Eagle Nebula. This region has been the subject of intensive spectroscopic (Hillenbrand et al. 1993; Evans et al. 2005), multiwavelength optical (Belikov et al. 2000) and infrared (Oliveira et al. 2005; Guarcello et al. 2007) surveys. No systematic study of the cluster photometric variability has ever been performed. The rich population of the O and B-type stars makes the cluster a very promising target for variability searches among young and massive stars. The immediate goal of the present work is to detect and characterize interesting objects showing photometric variations, especially on the short time-scale.

The paper is organized as follows. First, we described the photometric observations and transformation to the standard system (Sect. 2). Next, the calculation of membership probabilities are presented (Sect. 3). In Sect. 4 we provide a review of variable stars in NGC 6611, and in the following Sect. 5, we describe the supplementary photometry¹ used to the identification and classification of PMS stars. Finally, a brief summary and conclusions are given (Sect. 6).

2 UBVI_C PHOTOMETRY

2.1 Observations and Reductions

The observations of NGC 6611 were carried out with three telescopes located in Chile. Most of the observations were taken in no more than a few hours per night due to bad weather or as a background project. The observed fields are shown in Fig. 1.

We used the 1-m telescope at Cerro Tololo Inter-American Observatory (CTIO) operated by the SMARTS² consortium from June 19 to July 18 2008. This telescope is equipped with a 4064×4064 CCD camera that covers an area of the sky of $20' \times 20'$. We collected 380 frames in the V filter and 170 frames in the B filter.

During three nights in July 2008, three nights in August 2008, and four nights in March 2009, NGC 6611 was observed with the SMARTS 0.9-m telescope at CTIO. The 2048×2046 CCD camera covered $13.5' \times 13.5'$ area of the sky. We took 40 frames in the U filter, 200 in the B filter, 680 in the V filter and 100 in the I filter.

Finally, during several nights between May and July 2008 and between March and May 2009, we carried out observations with 1-m Swope telescope at Las Campanas Observa-

¹ The supplementary photometry for variable stars is available in electronic form.

² Small and Moderate Aperture Research Telescope System

Table 1. The coefficients of the photometric transformations with Eq. 1, 3, and 4 determined from photometry of Guarcello et al. (2007). The numbers in parentheses are the rms errors of the transformation coefficients with leading zeros omitted.

Telescope	a_1	b_1	σ_1	N_1	a_3	b_3	σ_3	N_3	a_4	b_4	σ_4	N_4
SWOPE	-0.058(2)	10.850(1)	0.029	920	1.220(10)	0.713(4)	0.080	725	0.918(3)	1.199(1)	0.036	920
CT-1m	0.052(6)	10.929(3)	0.042	718	0.880(7)	0.663(4)	0.053	718	-	-	-	-
CT-0.9m	0.056(5)	10.941(2)	0.043	573	0.966(7)	0.685(4)	0.039	389	1.054(4)	1.213(2)	0.039	573

Table 2. The coefficients of the photometric transformations with Eq. 2, 3, and 5 determined from photometry of Hillenbrand et al. (1993).

Telescope	a_2	b_2	σ_2	N_2	a_3	b_3	σ_3	N_3	a_5	b_5	σ_5	N_5
CT-0.9m	0.044(11)	10.967(4)	0.047	88	0.938(10)	0.588(3)	0.033	99	1.143(10)	-0.479(8)	0.045	63

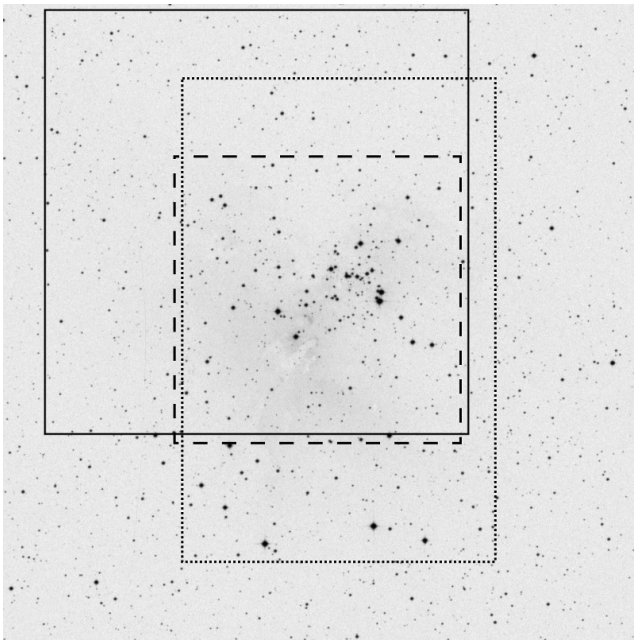


Figure 1. A $30' \times 30'$ fragment of the DSS-1 plate containing the observed fields of NGC 6611. Solid line shows the field observed with the 1-m CTIO telescope, dashed line – 0.9-m CTIO telescope, dotted line – 1-m Swope telescope.

tory, equipped with a 2048×3150 CCD camera covering a $14.8' \times 22.8'$ area of the sky. With the Swope telescope, we collected 810 frames in the V filter, 120 frames in the B filter and 100 frames in the I filter.

Observations from all telescopes were calibrated in a standard way. Profile and aperture photometry were derived by means of the DAOPHOT II package (Stetson 1987), and the differential magnitudes were calculated.

In total, we have detected 6038 stars but some have photometry of poor quality. Moreover, many stars were detected only on I filter frames.

2.2 Transformation to the standard system

UBV photometry of NGC 6611 was provided by Hillenbrand et al. (1993), while BVI_C photometry was published by Guarcello et al. (2007).

Unfortunately, there is no good agreement between B and V photometry for common stars. This problem was described by Guarcello et al. (2007), who found the difference between their own magnitudes and the ones of Hillenbrand et al. (1993) equal to -0.065 mag in the V and 0.018 mag in the B band. Since our observations were made in $UBVI_C$ bands, we used both photometric data to transform mean instrumental magnitudes and colours to the standard system. We used the following transformation equations:

$$V - v = a_1 \times (v - i) + b_1, \quad (1)$$

$$V - v = a_2 \times (b - v) + b_2, \quad (2)$$

$$B - V = a_3 \times (b - v) + b_3, \quad (3)$$

$$V - I_C = a_4 \times (v - i) + b_4, \quad (4)$$

$$U - B = a_5 \times (u - b) + b_5, \quad (5)$$

where v , b , i , and u denote the mean instrumental magnitudes from our photometry, and V , B , I_C , and U are the standard magnitudes. The coefficients obtained by means of the least-squares method are shown in Tables 1 and 2. In addition, these tables include the standard deviation of the residuals (σ) and the number of stars (N) used for the transformation. Transformations based on the photometry of Guarcello et al. (2007) were performed for each CCD camera independently (Table 1) after which the magnitude and colours of each star were averaged. In this way, we calculated V magnitudes and $(V - I_C)$ colour indices for 1900 stars and $(B - V)$ colour indices for 1598 stars. The colour-magnitude diagrams are shown in Fig. 2.

Photometry in the U band was taken only with the 0.9-m CTIO telescope. The coefficient transformations defined in Eq. (2), (3) and (5), were obtained from photometry of Hillenbrand et al. (1993) and are shown in Table 2. The colour-colour diagram for 319 stars is shown in Fig. 3. The symbols in Fig. 2 and Fig. 3 represent the variable stars we found, which are described in Sect. 4.

The resulting magnitudes and colours of the variable stars

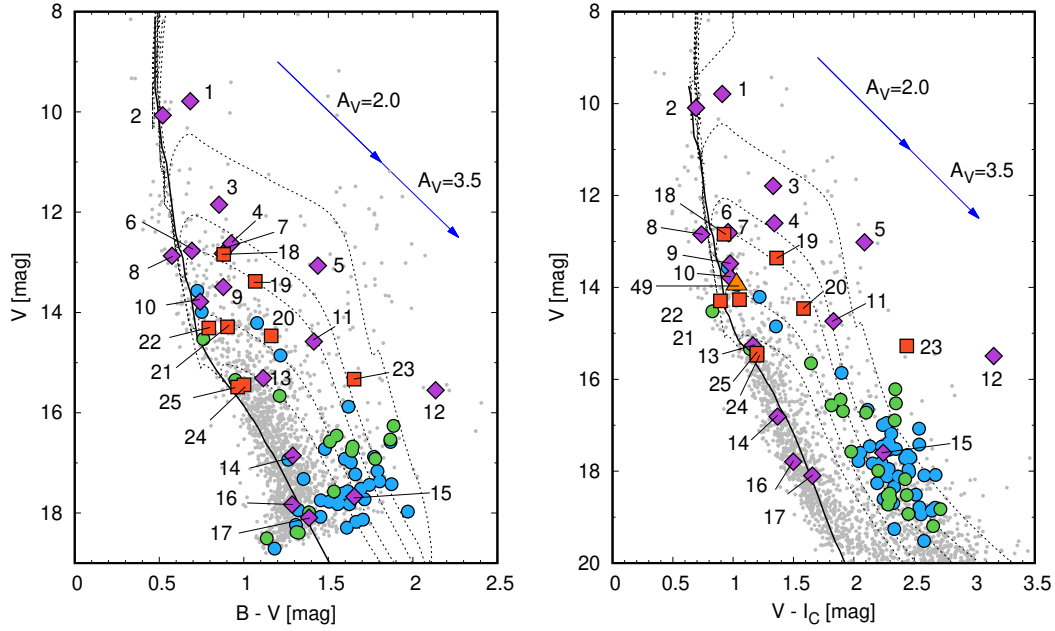


Figure 2. Variable stars in V vs. $(B - V)$ (left) and V vs. $(V - I_C)$ (right) colour-magnitude diagrams for the observed field. Symbols denote the variable stars found in this paper: pulsating stars (red squares), eclipsing stars (pink diamonds), other periodic variables (green), the remaining variables (blue) and H AeBe star (orange triangle). Some variables discussed in text are labeled with a number. The zero-age main sequence (ZAMS) relation (thick line) was taken from [Pecaut & Mamajek \(2013\)](#). The isochrones (dotted lines) for 0.1, 0.5, 1, 3, and 6 Myr were taken from [Bressan et al. \(2012\)](#). Following [Guarcello et al. \(2007\)](#) we assumed a distance $d = 1750$ pc, $A_V = 2.6$ mag and $R_V = 3.27$ and, which corresponds to $E(B - V) = 0.795$ mag and $E(V - I) = 0.994$ mag. Additionally, two extinction vectors for young ($A_V = 3.5$ mag) and for old ($A_V = 2.0$ mag) population ([Stoop et al. 2022](#)) adopting $R_V = 3.27$. and colour excess relation $E(B - V)/E(V - I) = 0.8$ ([Munari & Carraro 1996](#))

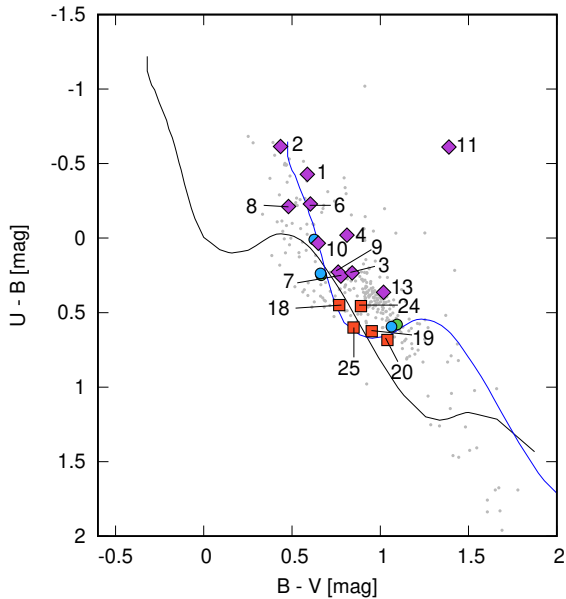


Figure 3. Variable stars in the $(U - B)$ vs. $(B - V)$ colour-colour diagram for the observed field. The symbols are the same as in Fig. 2. The black line represent the intrinsic relation for unreddened main-sequence stars taken from [Pecaut & Mamajek \(2013\)](#). The same relation for reddened stars with $E(B - V) = 0.795$ mag is plotted with the blue line. For the reddening line, $E(U - B)/E(B - V) = 0.72$ was adopted.

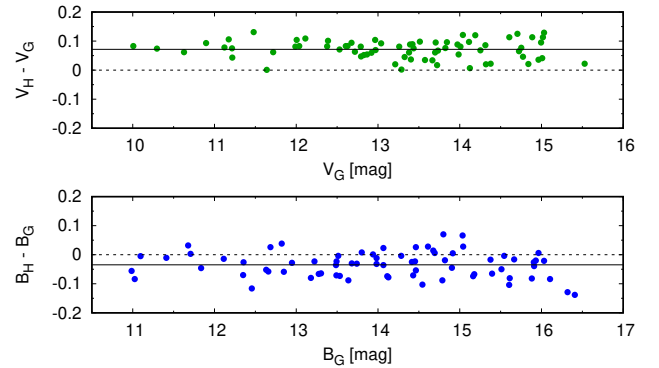


Figure 4. Difference between the magnitudes of [Hillenbrand et al. \(1993\)](#) (index 'H') and [Guarcello et al. \(2007\)](#) (index 'G') for the V (top) and B (bottom) magnitudes for common stars in the field of NGC 6611. The continuous lines represent the mean magnitude offset between the two samples.

are given in Table A1 in the Appendix. It is easy to see there are some differences between the $(B - V)$ colours derived from the photometry of [Guarcello et al. \(2007\)](#) (column 6) and [Hillenbrand et al. \(1993\)](#) (column 7). This is mainly due to some inconsistency in the V photometry published by both groups of authors. The differences in V and B magnitudes of the common stars, shown in Fig. 4, are 0.071 and -0.035 mag, respectively. Although, as a consequence of these differences, the magnitudes and colours we obtained are subject to systematic errors, and the colour-magnitude and colour-colour

diagrams proved useful in identifying the variability type of some stars.

3 MEMBERSHIP

The accurate determination of the probability of cluster membership is an important step in the study of cluster properties. The selection of cluster members based on proper motions for cluster and field stars was proposed by Vasilevskis et al. (1958). This method has been developed over the years (Sanders 1971, Zhao & He 1990, Uribe & Brieva 1994). The probability that the i -th star belongs to the cluster can be calculated from the following formula:

$$P_{\mu}(i) = \frac{n_c \cdot \phi_c^{\nu}(i)}{n_c \cdot \phi_c^{\nu}(i) + n_f \cdot \phi_f^{\nu}(i)}, \quad (6)$$

where n_c and n_f are, respectively, the normalized numbers of cluster and field stars ($n_c + n_f = 1$), and ϕ_c^{ν} and ϕ_f^{ν} are the frequency distribution functions for the cluster and field stars, defined as:

$$\phi_c^{\nu} = \frac{1}{2\pi\sqrt{(\sigma_{x_c}^2 + \epsilon_{x_i}^2)(\sigma_{y_c}^2 + \epsilon_{y_i}^2)}} \times \exp\left\{-\frac{1}{2}\left[\frac{(\mu_{x_i} - \mu_{x_c})^2}{\sigma_{x_c}^2 + \epsilon_{x_i}^2} + \frac{(\mu_{y_i} - \mu_{y_c})^2}{\sigma_{y_c}^2 + \epsilon_{y_i}^2}\right]\right\} \quad (7)$$

and

$$\phi_f^{\nu} = \frac{1}{2\pi\sqrt{(1-\gamma^2)}\sqrt{(\sigma_{x_f}^2 + \epsilon_{x_i}^2)(\sigma_{y_f}^2 + \epsilon_{y_i}^2)}} \times \exp\left\{-\frac{1}{2(1-\gamma^2)}\left[\frac{(\mu_{x_i} - \mu_{x_f})^2}{\sigma_{x_f}^2 + \epsilon_{x_i}^2} - \frac{2\gamma(\mu_{x_i} - \mu_{x_f})(\mu_{y_i} - \mu_{y_f})}{\sqrt{(\sigma_{x_f}^2 + \epsilon_{x_i}^2)(\sigma_{y_f}^2 + \epsilon_{y_i}^2)}} + \frac{(\mu_{y_i} - \mu_{y_f})^2}{\sigma_{y_f}^2 + \epsilon_{y_i}^2}\right]\right\}, \quad (8)$$

where μ_{x_i} and μ_{y_i} are the proper motions of the i -th star ($\mu_{x_i} = \mu_{\alpha} \cos \delta$ and $\mu_{y_i} = \mu_{\delta}$ of the i -th star) with errors ϵ_{x_i} and ϵ_{y_i} , respectively. The parameters μ_{x_c} and μ_{y_c} denote the cluster proper motion centre with dispersions σ_{x_c} and σ_{y_c} , while μ_{x_f} and μ_{y_f} stand for the proper motion centre for field stars with dispersions σ_{x_f} and σ_{y_f} , respectively. The correlation coefficient γ was calculated by

$$\gamma = \frac{(\mu_{x_i} - \mu_{x_f})(\mu_{y_i} - \mu_{y_f})}{\sigma_{x_f}\sigma_{y_f}} \quad (9)$$

(Sariya et al. 2012)

The proper motions of observed stars were taken from the Gaia Early Data Release 3 (Gaia EDR3; Gaia Collaboration et al. 2016, Gaia Collaboration 2020). They are shown in the left panel of Fig. 5. The mean proper motion of the cluster was calculated from the 30 stars with membership probability above 80% (Belikov et al. 1999). We obtained $\mu_{\alpha} \cos \delta = 0.241$ mas yr⁻¹ and $\mu_{\delta} = -1.658$ mas yr⁻¹ with standard deviation $\sigma_{\mu_{\alpha}} = 0.179$ and $\sigma_{\mu_{\delta}} = 0.231$, respectively. We assume that the cluster stars are within an ellipse with semi-axis equal to $3\sigma_{\mu_{\alpha}}$ and $3\sigma_{\mu_{\delta}}$ around the calculated centre (black cross in Fig. 5). Then, using the 995 stars located in this area, we calculated the mean proper motion of the cluster $\mu_{x_c} =$

0.224 and $\mu_{y_c} = -1.627$ mas yr⁻¹ with dispersions $\sigma_{x_c} = 0.244$ and $\sigma_{y_c} = 0.265$ mas yr⁻¹. Using the remaining 3122 stars, we calculated the mean proper motion of field stars $\mu_{x_f} = -0.164$ and $\mu_{y_f} = -2.536$ mas yr⁻¹ with dispersions $\sigma_{x_f} = 2.339$ and $\sigma_{y_f} = 3.023$ mas yr⁻¹. From these values, we calculated the frequency distribution functions ϕ_c^{ν} and ϕ_f^{ν} and the membership probability $P_{\mu}(i)$ for each star. The probabilities for the variable stars are shown in Table A1. As can be seen in the left panel of Fig. 5, most of our variable stars are located near the cluster centre and many of them are younger than 3 Myr (right panel of Fig. 5).

The Gaia EDR3 catalogue also contains parallaxes of stars. Using stars with membership probabilities greater than 80%, we derived the weighted average parallax of the cluster to be 0.56 mas. This corresponds to the distance of 1780 pc, which is consistent with the value obtained by Kuhn et al. (2019).

4 VARIABLE STARS

The search for variable stars was performed on merged data. Prior to merging, data sets from each observatory were prepared: the outliers were removed using 3σ -clipping and the mean magnitude was subtracted. The data-sets were combined for each filter separately. In the next step, Fourier spectra up to 80 d⁻¹ were calculated from the V -filter data, as they have the best time coverage. In addition, the light curves, periodgrams, and phased light curves for all stars were visually inspected. In total, we found 95 variable stars. Their location in schematic map of the observed field is shown in Fig. 6. Some variable stars discussed in the paper are labelled with our identification number. The cross-identification with the numbering provided by the WEBDA³ database is shown in Table A1 of the Appendix. If we refer to the WEBDA number in the paper, we preceded it with letter 'W'.

4.1 Pulsating stars

Among 95 variables found in the observed field, eight are candidates for δ Scuti-type stars. The parameters of the sinusoidal terms (frequency, f_i , semi-amplitude, A_i , and phase, ϕ_i), listed in Table 3, were derived by fitting the formula:

$$\langle m \rangle + \sum_{i=1}^n A_i \sin(2\pi f_i(t - T_0) + \phi_i) \quad (10)$$

to the analyzed differential magnitudes. In Eq. (10) $\langle m \rangle$ is the mean differential magnitude, n is the number of terms, t is the time elapsed from the initial epoch $T_0 = HJD2454000$. Additionally, for each frequency, we calculated signal-to-noise (S/N) where S is the amplitude of the frequency and N is the average noise level in an amplitude spectrum of the residuals.

The most luminous object among δ Scuti candidates, classified as F0 III-V star (Neubauer 1943), is star #18 (W135). It is not a member of the cluster (Tucholke et al. 1986, Belikov et al. 1999, Table A1). The Fourier spectrum (Fig. 7) reveals a frequency of 5.89911 d⁻¹. This result is consistent with a periodicity of 0.169567 d reported by Heinze et al. (2018). We found six other terms in successive steps of prewhitening.

³ The WEBDA database is available on a web page <http://webda.physics.muni.cz>.

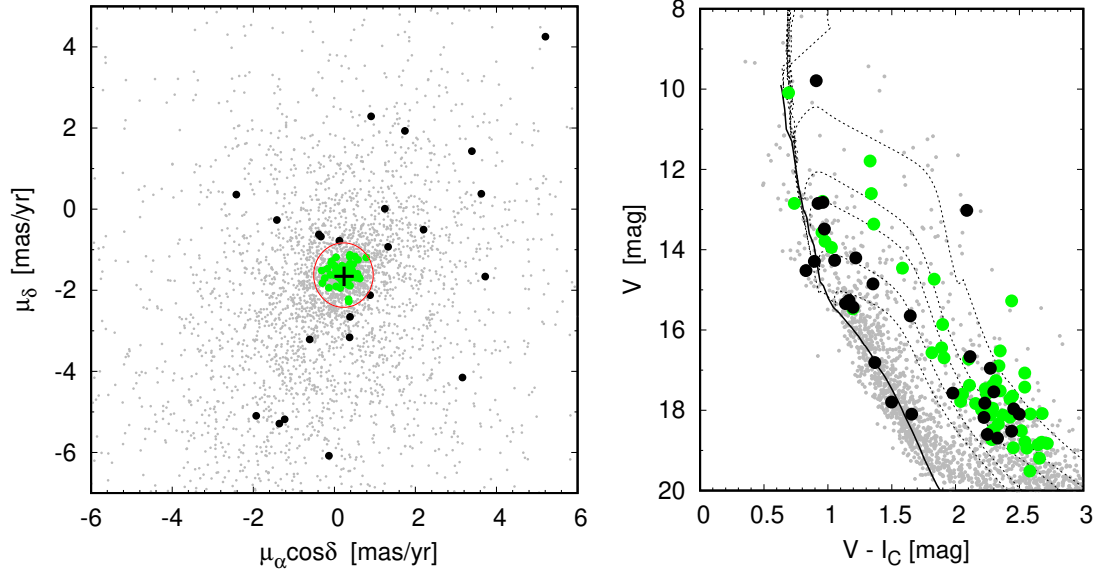


Figure 5. *Left:* Distribution of proper motions for about 4000 stars in the observed field. *Right:* Colour-magnitude diagram for about 4000 stars in the observed field. Green circles represent variable stars falling within the oval area around the mean proper motion of NGC 6611 (black cross), black circles – the remaining variable stars. The isochrones (dotted lines) for 0.1, 0.5, 1, 3, and 6 Myr were taken from [Bressan et al. \(2012\)](#).

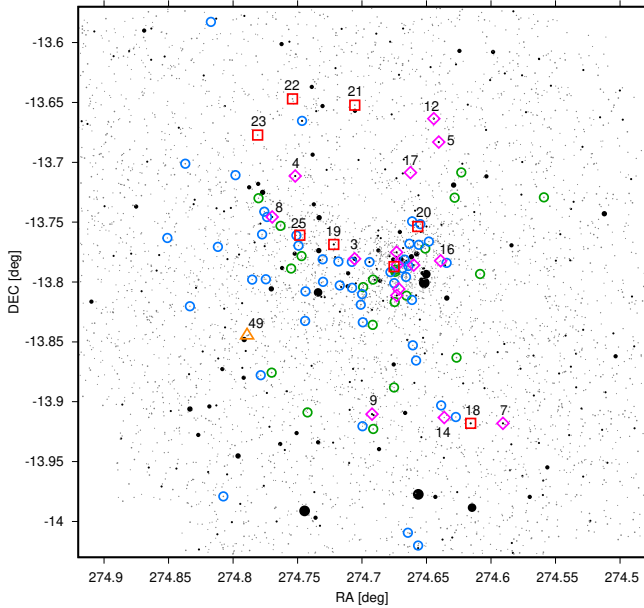


Figure 6. Schematic map of the observed field. Variable stars are colour-coded: pulsating stars (red squares), eclipsing stars (pink diamonds), other periodic variables (green circles), the remaining variables (blue circles) and H Ae Be star (orange triangle). Some variables discussed in the text are labelled.

The two with the lowest frequencies are presumably not due to pulsations but instrumental effects. They are denoted as f_x and f_y . Four other frequencies $f_4 - f_7$ are almost equally high as their corresponding alias frequencies. It means that the true frequency may differ by 1 d^{-1} . The multiperiodicity and spectral type clearly indicate a δ Scuti-type star.

Another candidate for a δ Scuti type star is #19 (W374).

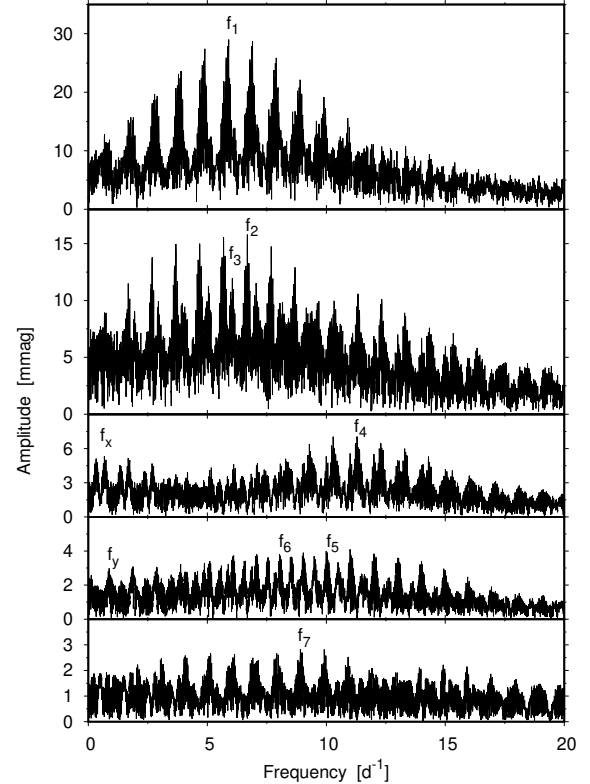


Figure 7. Fourier frequency spectrum of the V -filter data of the δ Scuti candidate, star #18, at four steps of prewhitening.

The variability was reported by [de Winter et al. \(1997\)](#), who classified the star as F2e. After prewhitening with a dominant frequency ($f_1 = 7.747645$), two other frequencies of 2.56 and 3 d^{-1} (marked as f_x and f_y in Fig. 8) are clearly seen in the

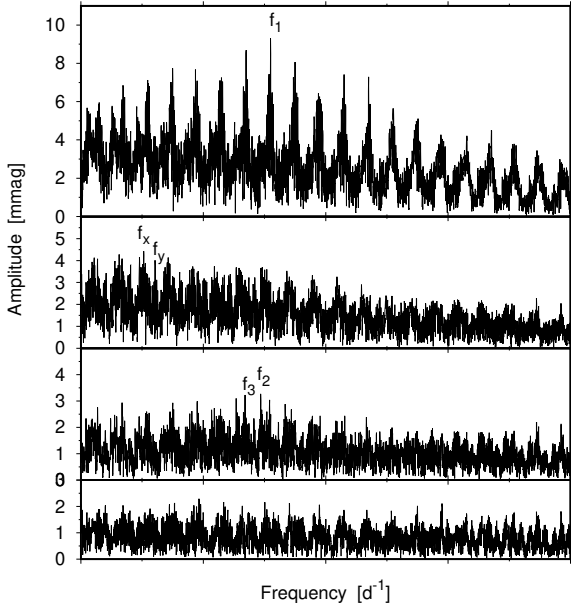


Figure 8. Fourier frequency spectrum of the V -filter data of the δ Scuti candidate, star #19: original data (top) and three steps of prewhitening.

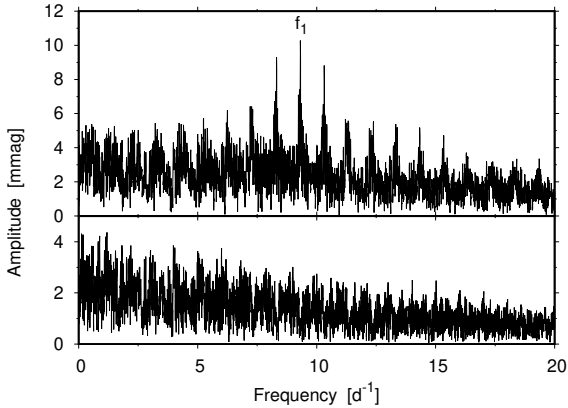


Figure 9. Fourier frequency spectrum of the original V -filter data of the δ Scuti candidate, star #20 (upper panel), and after prewhitening with f_1 and its three harmonics (lower panel).

Fourier spectrum. The corresponding phase diagrams, however, indicate that these frequencies are not caused by pulsations. The removal of these frequencies led us to find another two peaks with frequencies of $f_2 = 7.34435$ and $f_3 = 6.70819$ d^{-1} . Based on the Gaia proper motions, we calculated a membership probability of 94.8%, which is inconsistent with previous determinations of 0% derived by Tucholke et al. (1986) and Belikov et al. (1999).

An interesting star appears to be #20 (W221). The Fourier spectrum (Fig. 9a) reveals a single periodicity with a frequency of 9.318127 d^{-1} , typical of δ Scuti-type stars. The spectral type of this star estimated by Walker (1961) is G. The star was later found to be B8Ve type with broad lines (Hillenbrand et al. 1993). This spectral type, however, seems to be too early for a δ Scuti star. The membership probability we found is equal to 97.0%. The position in the colour-colour

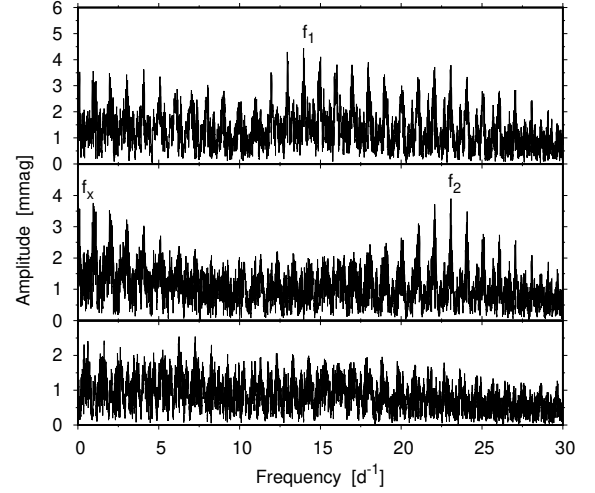


Figure 10. Fourier frequency spectrum of the V -filter data of the δ Scuti candidate, star #21: original data (top), after removing f_1 (middle), after removing f_1 , f_2 and f_x (bottom).

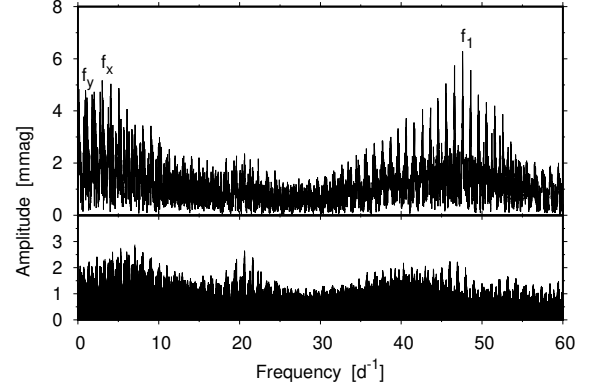


Figure 11. Fourier frequency spectrum of the V -filter data of the δ Scuti candidate, star #22: original data (top), after removing f_1 , f_x and f_y (bottom).

and colour-magnitude diagrams indicates that if the star is a member of NGC 6611, it cannot be B8 V type.

The next δ Scuti candidate is star #21 (W347) classified as A7 III (Martayan et al. 2008). Two frequencies are clearly seen in the Fourier spectrum (Fig. 10). The low-frequency peak labelled as f_x probably comes from instrumental effects. This star is not a member of the cluster (Table A1).

The other four candidate δ Scuti stars (#22, #23, #24, and #25) have no determined spectral types. Their Fourier spectra are shown in Figs. 11–14, and the parameters of the sinusoidal fits are given in Table 3. The frequencies that are not due to pulsations (likely instrumental) are labelled as f_x and f_y . We found two frequencies in Fourier spectra of variable #23 and #25. The membership probability of stars #22 and #24 is 0, whilst for stars #23 and #25, it is more than 90%. The variable #24 has a visual companion separated by $0.872''$ (Duchêne et al. 2001). This star was marked as ‘DSCT/GDOR/SXPHE’ in the in the Gaia DR3 variability catalogue Gaia Collaboration (2022).

If these four δ Scuti stars are cluster members, then they should be in the pre-main sequence (PMS) state of

Table 3. Parameters of sinusoidal fits to the V -filter differential magnitudes of eight δ Scuti-type candidates detected in NGC 6611. Numbers in parentheses denote the r.m.s. errors of the preceding quantities with the leading zeroes omitted. The S/N is the signal-to-noise, σ_{res} is the standard deviation of residuals and N_{obs} is the number of observations. The frequencies not reliable due to aliasing problem are marked with an asterisk.

Star #	N_{obs}	Frequency [d ⁻¹]	f_i	A_i [mmag]	ϕ_i [rad]	$T_{\text{max}} - T_0$ [d]	S/N	σ_{res} [mmag]	Spectral type	Other name
18	894	5.899130(18)	f_1	28.5(3)	1.18(1)	898.0385(2)	69.6	4.8	FOIII/V	W135
		6.683535(32)	f_2	15.0(2)	1.32(2)	898.1426(4)	36.7			
		6.089909(54)	f_3	10.4(2)	5.01(2)	898.0557(6)	25.9			
		11.291034(54)	f_4^*	6.7(2)	1.37(3)	898.0813(5)	16.5			
		0.67443(10)	f_x	5.2(2)	1.35(5)	898.636(12)	12.9			
		10.998562(90)	f_5^*	6.2(3)	1.02(4)	898.0952(6)	15.2			
		8.49109(13)	f_6^*	4.0(2)	5.05(6)	898.0772(11)	9.6			
19	1424	0.94842(14)	f_y	3.4(2)	5.0(1)	897.981(16)	8.1	6.4	F2e	W374
		8.91439(14)	f_7^*	3.6(3)	0.87(7)	898.1277(13)	9.0			
		7.747645(42)	f_1	9.4(3)	3.78(3)	777.0531(07)	19.8			
		2.564905(89)	f_x	4.0(3)	5.92(9)	777.0190(44)	8.4			
		3.03159(13)	f_y	3.2(3)	2.45(9)	776.9201(49)	6.7			
		7.34435(11)	f_2	2.8(3)	2.51(9)	776.9944(21)	6.1			
		6.70819(11)	f_3	3.2(3)	0.54(9)	777.0949(21)	7.0			
20	1708	9.318127(46)	f_1	10.6(4)	4.50(4)	804.9010(7)	13.2	12.4	B8Ve	W221
21	1134	13.95823(11)	f_1	3.8(4)	5.0(1)	828.4212(11)	6.5	9.3	A7III	W347
		23.07700(12)	f_2	3.6(4)	2.36(11)	828.4570(7)	6.1			
22	1115	47.60165(8)	f_1	5.7(4)	5.35(7)	829.2947(2)	8.6	10.3		W451
		3.01478(12)	f_x	6.0(4)	1.01(8)	829.3135(42)	8.7			
		0.89815(11)	f_y	5.8(5)	3.63(9)	829.428(16)	8.6			
23	1132	8.126086(74)	f_1	8.9(5)	4.17(6)	828.7480(12)	11.5			W491
		0.89012(11)	f_x	5.9(5)	5.63(9)	828.499(16)	8.1			
		9.724230(14)	f_2^*	4.3(5)	4.65(12)	828.7291(20)	6.0			
24	1844	15.486392(93)	f_1	7.6(6)	5.55(8)	807.6587(08)	7.9	17.9		W270
		0.866011(90))	f_x	7.8(6)	5.51(8)	807.485(14)	8.1			
25	1858	46.749073(63)	f_1	9.5(5)	3.26(5)	808.7495(1)	12.2	15.5		W435
		0.05769(13)	f_x	4.9(6)	5.31(11)	812.35(32)	6.3			
		44.14812(10)	f_2	5.9(5)	2.94(9)	808.7390(3)	7.6			

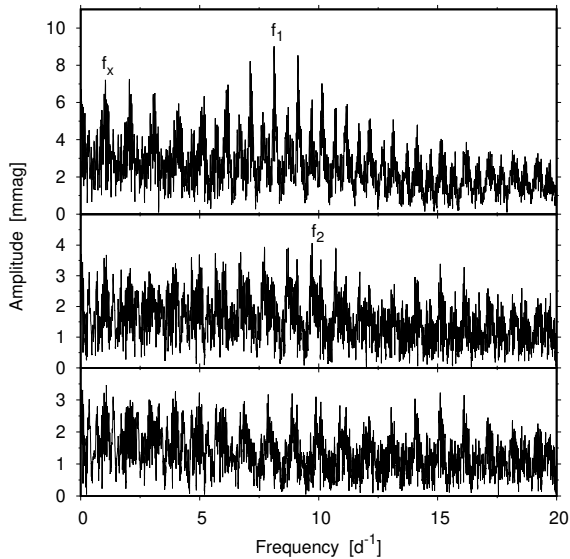


Figure 12. Fourier frequency spectrum of the V -filter data of the δ Scuti candidate, star #23: original data (top), after removing f_1 and f_x (middle), after removing f_1 , f_x and f_2 (bottom).

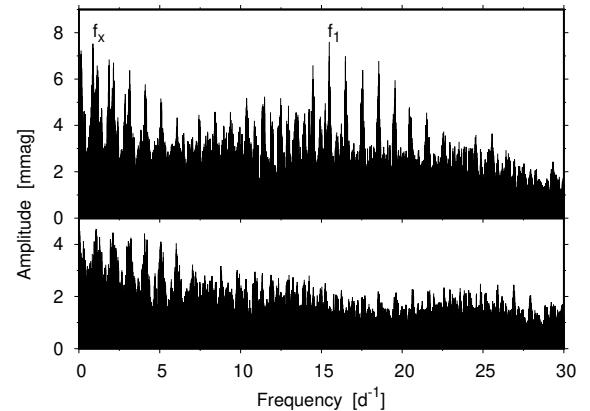


Figure 13. Fourier frequency spectrum of the V -filter data of the δ Scuti candidate, star #24: original data (top), after removing f_1 and f_x (bottom).

evolution. To verify this, we marked these stars in the Hertzsprung–Russell (HR) diagram together with the other

δ Scuti stars (Fig. 15). The values of M_V and $(B - V)_0$ were calculated assuming $A_V = 2.6$ mag, $E(B - V) = 0.795$ mag and a distance modulus equal to 11.215 mag. The black dots in Fig. 15 represent PMS δ Scuti candidates taken from the work of Zwintz (2008). The author noted that the PMS pulsators occupy the same instability region in the HR diagram as classical δ Scuti stars, which are indicated by the grey dots

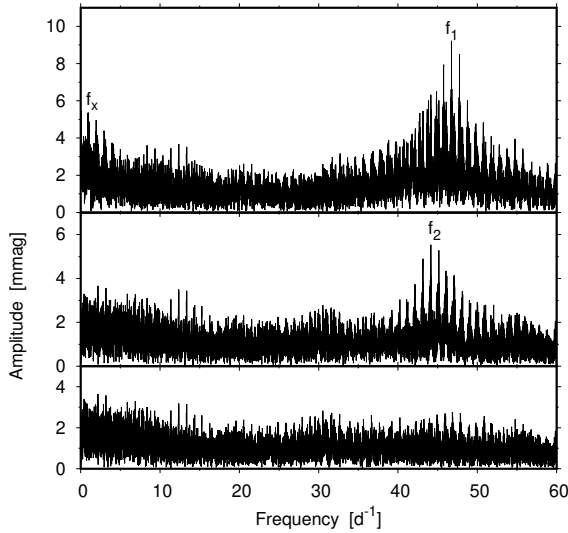


Figure 14. Fourier frequency spectrum of the V -filter data of the δ Scuti candidate, star #25: original data (top), after removing f_1 and f_x (middle), after removing f_1 , f_x and f_2 (bottom).

in Fig. 15. We derived $(B-V)_0$ from the $(b-y)_0$ colours published by Rodríguez & Breger (2001)⁴ using transformation given by Caldwell et al. (1993). The instability strip (dotted line) and ZAMS (black solid line) were also transformed from the data of Rodríguez & Breger (2001). The membership probability of four δ Scuti candidates is greater than 90%. Three of them, marked as red dots in Fig 15, lie inside the δ Scuti instability region. The fourth star, #23, has $(B-V)_0 = 0.8578$ mag that places it far from the instability strip. If this star is indeed a δ Scuti-type variable, it is not a member of the cluster. At this time, we cannot exclude this star to be a δ Scuti-type star. The second frequency we found is questionable because it is close to the noise level. The variability of this star may be caused by spots.

4.2 Binary stars

In the observed field, we found 17 binary stars. Due to the saturation, we were unable to analyze a well-known spectroscopic binary, HD 186183 (W412, QR Ser), which is a probable eclipsing star (Watson et al. 2006). The analysis of another binary star, BD $-13^\circ 4923$ (W175), reveals no eclipse. This result confirms the low inclination predicted by Sana et al. (2009). The next interesting binary discovered recently by Shultz et al. (2021), BD $-13^\circ 4937$ (W601), was outside the field of view in most of our images.

The orbital periods, minimum light times, and variability ranges are listed in Table 4. We were unable to find the orbital period of one eclipsing star, #11. This star’s light curve is shown in Fig. 16. The phased light curves of the other fifteen binaries are shown in Fig. 18.

The brightest eclipsing system in our sample is star #1 (BD $-13^\circ 4929$, W314). The binary nature was noted by Trumpler (Walker 1961) and was detected by Bosch et al. (1999) and Evans et al. (2005). This star was later discovered by Sana et al. (2009) to be a spectroscopic triple star (SB3) composed

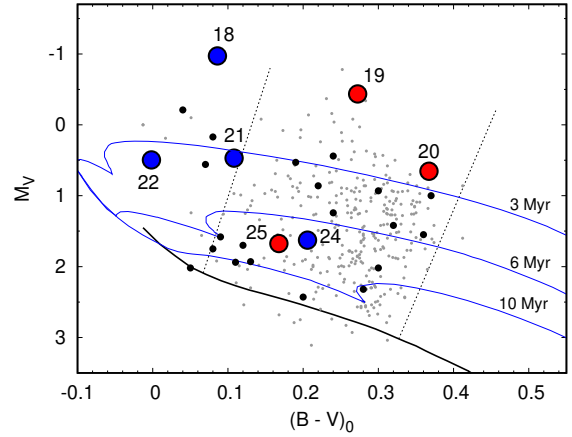


Figure 15. Position of δ Scuti candidates in HR diagram: cluster members (red dots) and non-members (blue dots). Additionally, 20 pulsating PMS stars taken from Zwintz (2008) are plotted. The ZAMS (black solid line), the borders of the classical δ Scuti instability strip (dotted lines) and classical δ Scuti stars (grey dots) were transformed from the data of Rodríguez & Breger (2001). The blue line represents isochrones for 3, 6, and 10 Myr taken from Bressan et al. (2012).

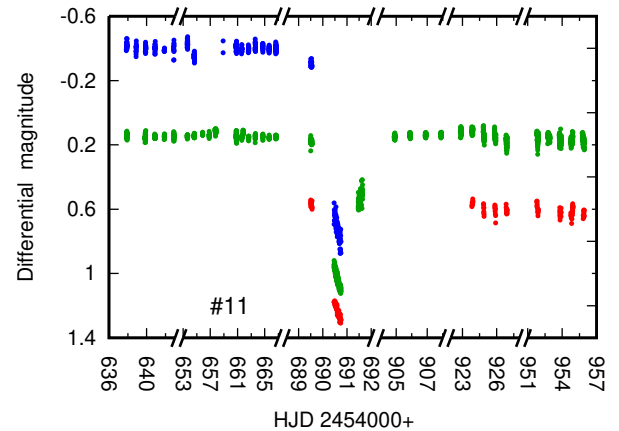


Figure 16. Light curve of eclipsing system #11. The blue, green and red dots represent B , V , and I_C data, respectively.

of a short-period binary (B0.5V+B0.5V) and an O7V star. The authors, however, found no evidence that the O-type star is gravitationally bound with the binary pair. We discovered it to be an eclipsing system with an orbital period equal to 1.475091 d.

Star #2 (BD $-13^\circ 4928$, W280) was known as a Be star with a spectral type B0.5:V:ne (Hiltner & Iriarte 1955). Hillenbrand et al. (1993) classified this star as O9.5 V with broad lines. Radial velocities derived by Bosch et al. (1999) showed no significant variations, and the authors considered the star to be constant. We found this star to be an eclipsing system with an orbital period of 3.692046 d (Fig. 17). Sana et al. (2009) calculated the radial velocities for eleven lines, but they do not agree with each other. Using our period, we phased each set of radial velocities. We found the best agreement with the light curve for radial velocities derived from He I 4471 Å and He II 4686 Å lines. These radial velocities are shown in bottom panel of Fig. 17.

⁴ <http://www.iaa.es/~eloy/dsc00.html>

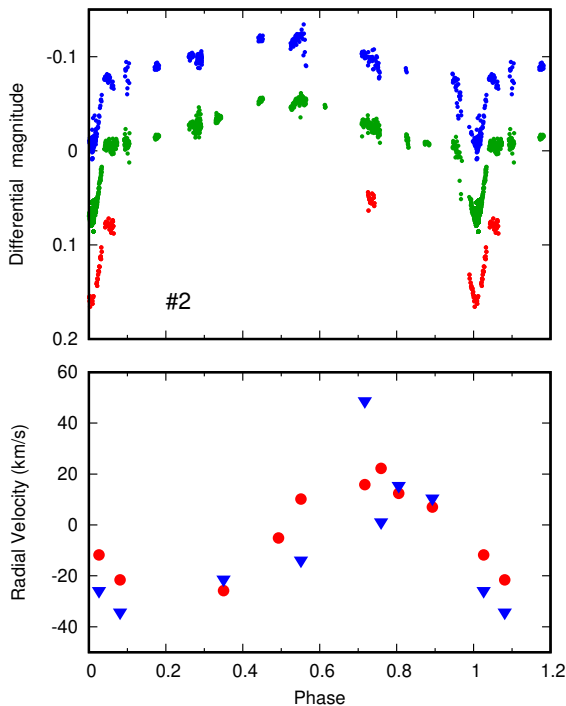


Figure 17. *Top:* Phase diagrams of the BVI_C observations of the eclipsing system #2, phased with $P = 3.692046$ d. *Bottom:* Radial velocities for He I 4471 Å (red dots) and He II 4686 Å (blue triangles) derived by Sana et al. (2009).

Another eclipsing system, star #3 (W343), was classified as B1 V by Hillenbrand et al. (1993) and Wolff et al. (2007). This system was found to be an EA-type binary with an orbital period of 1.15023 d (Watson et al. 2006). Duchêne et al. (2001) reported a visual companion of the star at a distance of 1.449". The rotational velocity ($v \sin i$) of the star was found to be 300 km s^{-1} (Wolff et al. 2007). The BVI_C data phased with period of 1.1500665 d are shown in Fig. 18.

The next binary system we investigated was star #4 (W444, ALS 15393). The spectral type B1.5 V determined by Hillenbrand et al. (1993) was confirmed by Evans et al. (2005) and Wolff et al. (2007). The radial velocity measured by Evans et al. (2005) is equal to 7 km s^{-1} , which is close to the average radial velocity of the cluster (10 km s^{-1}). The rotational velocity $v \sin i$ of the star #4 is equal to 133 km s^{-1} (Wolff et al. 2007). Guarcello et al. (2009) stated that the star is an X-ray source with no infrared excess, i.e. it is a candidate for a star without a disk, while Guarcello et al. (2012), based on optical and infrared colours, classified the star as a background object. The membership probability we found from the Gaia proper motions (Sect. 3) is 88%. This probability is in good agreement with the value of 70% determined by Belikov et al. (1999). In catalog of variable stars measured by ATLAS (Asteroid Terrestrial-impact Last Alert System), this star was classified as ‘dubious’ with a period of 2.533454 d (Heinze et al. 2018). The light curve phased with a period 2.533757 d is shown in Fig. 18. The shape and small amplitude indicate that the star may be an ellipsoidal variable. The system may be also EW-type binary with very small orbital inclination.

The next eclipsing binary is star #5 (W188), classified as B0 V (Hillenbrand et al. 1993). Duchêne et al. (2001) found

a visual companion to this star at $0.543''$ with an estimated mass of $2.4\text{--}2.6 M_{\odot}$. Only a few points were detected during the two nights covering the eclipse, and thus we have determined a rather uncertain orbital period of 7.5956 d.

Star #6 (W227) was classified as an emission-line star of spectral type B1.5 Ve (Hillenbrand et al. 1993). The star was found later to be a B2 V star (Evans et al. 2005). Duchêne et al. (2001) discovered a visual companion at the distance of $0.538''$ with an estimated mass of $0.7 M_{\odot}$. The variability of the star with period of 2.522625 d was announced by Heinze et al. (2018). We found it to be an Algol type eclipsing system with an orbital period of 2.5224756 d. The phase diagram is shown in Fig. 18.

Next binary system found in the observed field is star #8 (W472). The star was classified as B3 Ve by Hillenbrand et al. (1993). The emission in $H\alpha$ line has not been confirmed by other authors (Herbig & Dahm 2001, Evans et al. 2005), but they suggest that the small emission in $H\alpha$ line may be due to the emission in nebula. Evans et al. (2005) classified it as B3 V star with a companion. The binary nature of that star was confirmed by Martayan et al. (2008). The authors derived the following fundamental parameters: $T_{\text{eff}} = 13000 \text{ K}$, $\log g = 3.2$ and $V \sin i = 121 \text{ km d}^{-1}$. They estimated the mass to be $M/M_{\odot} = 5.8$, the luminosity $\log L/L_{\odot} = 3.40$, and the radius $R/R_{\odot} = 10.1$. The age of 73 Myr that they obtained indicate that the star is not a member of the cluster. However, based on the proper motions from Gaia, we calculated that the membership probability is equal to 96.4%. In the catalog of variable stars measured by ATLAS (Jayasinghe et al. 2018), the authors provide a variability period of 1.806230, although they classified the star as irregular. We found periodic variations of this star with a frequency of $f_1 = 0.553616 \text{ d}^{-1}$, which corresponds to the period of 1.806307 d. The peculiar light curve, shown in Fig. 18, reveals no eclipse. Since the secondary minimum is shifted from phase 0.5, the system most likely has an eccentric orbit.

Star #9 (W310) is another binary system we have found. Hillenbrand et al. (1993) reported that the spectrum is a composite with features typical for B and G-type stars. The emission likely originates from circumstellar matter. The orbital period we derived is 0.392850 d, and we believe the star is not a cluster member.

For the star, #10 (W262, ALS 15370), it was classified by Hillenbrand et al. (1993) as Ae, whilst de Winter et al. (1997) classified it as a B7 star without any emission lines. The light curve (Fig. 18) indicates, the star may be obscured by surrounding matter.

The orbital period of the EW-type binary #13 (W258) has already been determined by Watson et al. (2006). The period is consistent with our value of 0.412470 d. This star and four other eclipsing binaries, #7, #14, #16, and #17, are not cluster members. As can be seen in Fig. 18, the phase coverage of star #5, #7, and #12 is incomplete, and therefore, their periods may be uncertain.

The frequencies corresponding to the periods of our five binary stars (star #1, #3, #7, #13, and #17) were recently published in the Gaia DR3 variability catalogue Gaia Collaboration (2022). For two other binaries (star #6 and #16), the value of the frequency published by the authors was two times lower compared to our result.

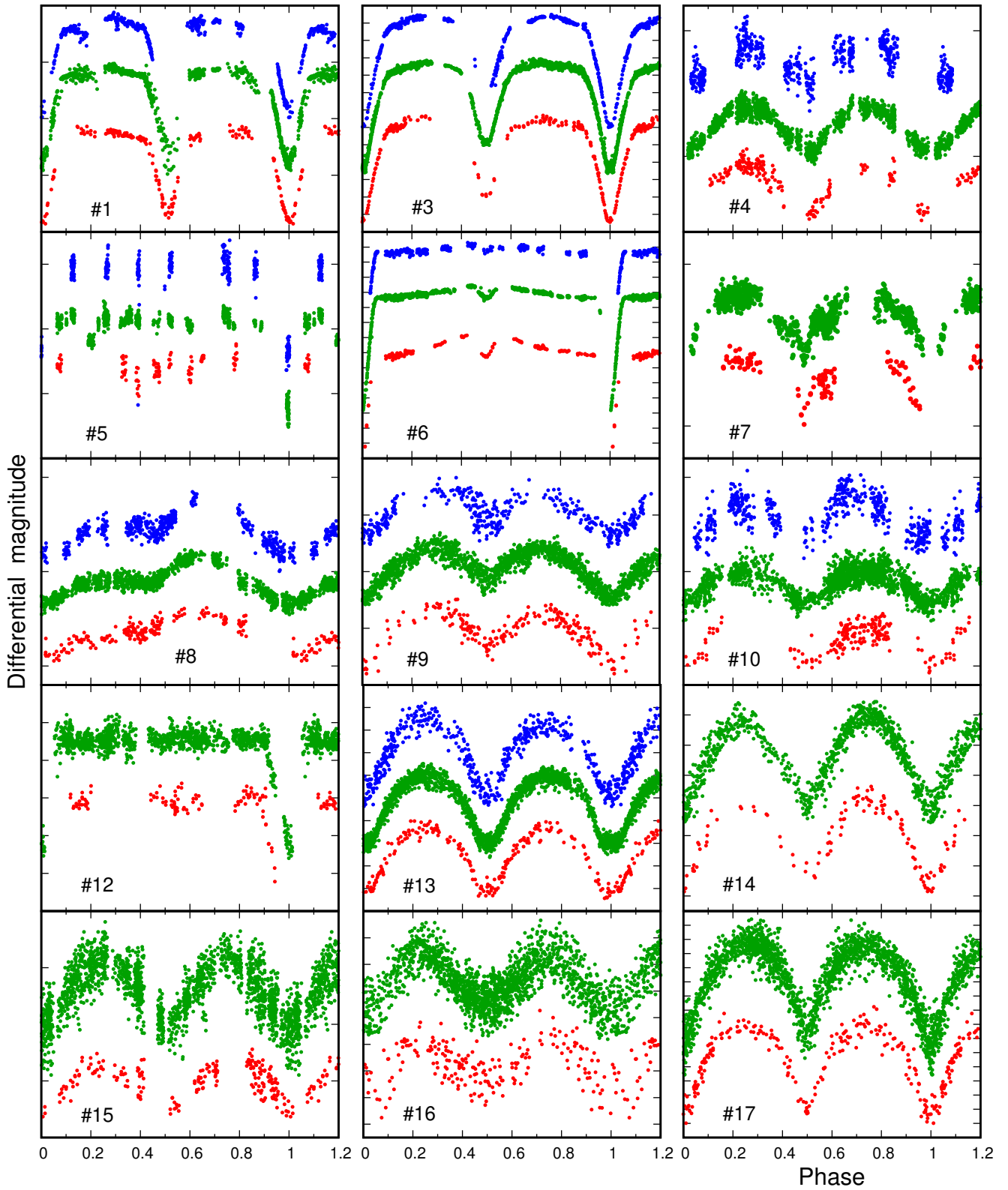


Figure 18. Phased light curves of fifteen binary stars in NGC 6611. The blue, green and red dots represent the B , V , and I_C data, respectively. Ordinate ticks are separated by 0.1 mag.

Table 4. The parameters of binary stars in the field of NGC 6611. Numbers in parentheses denote the r.m.s. errors of the preceding quantities with the leading zeroes omitted.

star #	Period [d]	$T_{\min} - T_0$ [d]	ΔV [mag]
1	1.475091(20)	784.494(88)	0.18
2	3.692046(56)	775.428(14)	0.12
3	1.1500862(13)	784.8521(46)	0.61
4	2.533697(37)	783.673(49)	0.035
5	7.59561(38)	784.21(56)	0.16
6	2.522476(7)	786.0860(44)	~ 0.8
7	1.530347(39)	785.715(91)	~ 0.05
8	1.806307 (36)	785.5984(36)	0.05
9	0.392850(1)	784.2626(16)	0.087
10	1.169840(13)	785.699(71)	0.034
11	–	~ 690.76	~ 1
12	1.581702(15)	784.8095(56)	0.28
13	0.4124697(4)	784.550(20)	0.31
14	0.348772(1)	784.029(12)	0.30
15	2.206034(52)	783.50(23)	0.233
16	0.340387(2)	784.173(11)	0.23
17	0.2721959(4)	783.9597(26)	0.70

4.3 Other periodic variables

We found 21 other periodic variables in the observed field. Unfortunately, these stars have no spectral classification. The periods, times of the maximum light and V -filter amplitudes are given in Table 5. The phased light curves of these stars are online in the electronic table in Appendix Fig. A1. Only four stars, #26, #27, #28, and #46 are not cluster members. The periods, the amplitudes and the shape of light curves in combination with their position in colour-magnitude diagram indicate that these stars may be WTTS stars. The light variations of WTTS stars are mainly caused by cool spots rotating around the stars. In order to check for other type of light variations in these stars, such as flares, we subtracted the changes with main frequency from the original light curves. However, we did not find any additional variability.

Fifteen stars in this group have been identified as X-ray sources without infrared excess (Guarcello et al. 2009). One of them, #46, and three other stars (#29, #33, and #44) were classified by Guarcello et al. (2012) as disk-bearing stars, while the rest as disk-less objects. Similar to NGC 2244 (Michalska 2019), all periodic cluster members have periods larger than one day. However, in some young open clusters, such as NGC 2282 (Dutta et al. 2018) or Stock 8 (Lata et al. 2019), a large fraction of the periodic variables have periods shorter than one day.

The distribution of rotation periods and their correlation with other stellar properties, such as mass, age, colour, have been studied by many authors. Some of them found that the distribution of rotation periods depends on mass and is unimodal for lower mass stars ($\leq 0.25M_{\odot}$) rotating faster than higher mass stars, and bimodal for more massive stars ($\geq 0.25M_{\odot}$) (Herbst et al. 2001 in Orion Nebula Cluster, Lamm et al. 2005 in NGC 2264). On the contrary, others (e.g. Henderson & Stassun 2012 in NGC 6530) have found that the rotation periods have a unimodal distribution and that the lower mass stars rotate slower on average. To check the dependence of periods on mass for our stars, we

Table 5. Parameters of 21 periodic variable stars found in the observed field determined from the V -filter observations ($T_0 = \text{HJD}2454000$). The numbers in parentheses denote the r.m.s. errors of the preceding quantities with the leading zeroes omitted.

Star	Period [d]	$T_{\max} - T_0$ [d]	ΔV [mag]
26	0.462019(07)	784.2858(27)	0.024
27	1.19924(27)	784.5428(74)	0.038
28	0.885414(30)	784.3877(38)	0.049
29	7.09957(94)	792.583(19)	0.163
30	4.96183(28)	787.6240(67)	0.304
31	2.76215(15)	787.0732(80)	0.143
32	2.86626(27)	786.896(14)	0.083
33	5.48703(56)	786.9072(14)	0.221
34	2.313617(78)	786.0491(47)	0.196
35	1.262206(59)	784.9040(44)	0.102
36	1.219393(37)	785.2882(36)	0.251
37	2.69119(22)	785.072(10)	0.303
38	5.219092(91)	782.543(25)	0.204
39	3.77175(39)	785.213(15)	0.306
40	5.29819(58)	787.854(15)	0.449
41	3.07131(56)	785.510(18)	0.313
42	1.154089(37)	784.9332(43)	0.357
43	1.134087(93)	784.030(11)	0.174
44	2.17628(24)	786.529(12)	0.308
45	1.34165(11)	784.3147(77)	0.418
46	1.56272(13)	784.8237(92)	0.372

have drawn our periodic variables in the colour-magnitude V vs. $(V - I)$ diagram. The objects are superimposed on the evolutionary tracks taken from Bressan et al. (2012). The colours of the symbols from light to dark green indicate the periods from the shortest to the longest. Three stars with $V - I < 1.8$ mag are not cluster members. The remaining stars are distributed uniformly in the wide range of masses. We did not observe any correlation between variability period and age. However, the statistics of our sample is too poor to draw conclusions about correlation between mass and period. Moreover, the magnitudes and colours of the stars would need to be determined more precisely first, since (as we mentioned in Sect. 2.2) we had some problems with the transformation to the standard system. More properties of these variables are discussed in Sect. 5.4.

4.4 Irregular variables

In addition to the periodic variables described in Sects. 4.1–4.3, we found 49 irregular variables. The membership probabilities determined from the Gaia proper motions (Sect. 3) indicate that ten of these stars are non-members. The light curves are available online in the electronic version in Appendix Fig. A2. As can be seen in these figures, the range of variability is from 0.1 mag (#47, #48) to more than one magnitude (#58, #78, #81, #94, #95). Their position in V vs. $(V - I_C)$ diagram (Fig. 2) indicates that many of them are young (0.1–3 Myr) PMS stars. As we mentioned in the introduction, the irregular light variations of PMS stars are associated with unstable accretion from the circumstellar disk, causing hot spots, obscuration by surrounding matter, and rotation of a star with asymmetrically distributed cool and hot spots (Herbst et al. 1994). The photometric variability

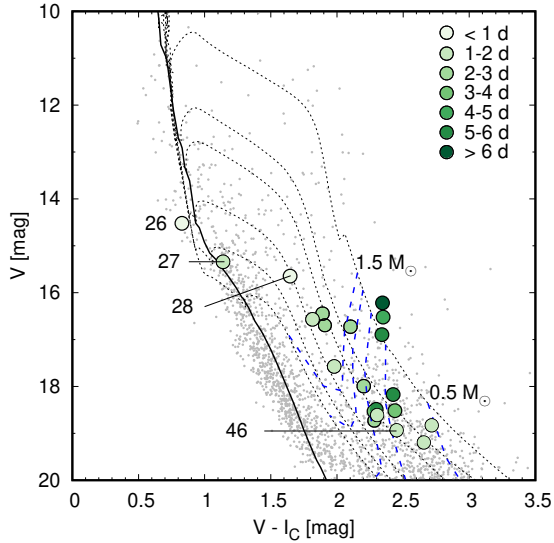


Figure 19. Position of periodic variables in the colour-magnitude diagram. The ZAMS relation for $Z=0.02$ (thick line) was taken from [Pecaut & Mamajek \(2013\)](#). The symbols denote the ranges of periods. Non-members are labeled with number. The isochrones (dotted lines) for 0.1, 0.5, 1, 3, 6, and 10 Myr and mass tracks for 0.5, 0.75, 1, 1.25, and 1.5 M_{\odot} (dashed blue lines) were taken from [Bressan et al. \(2012\)](#). We adopted the mean values of $E(V - I_C) = 0.994$ mag, $A_V = 2.6$ mag and $(m - M_V)_0 = 11.215$ mag.

of PMS stars may be caused by flares. The typical feature of flares is fast rise of light and slow, exponential decay. In order to find this phenomenon, all light curves were carefully inspected by eyes prior and after rejection of outstanding data points. However, we found no evidence of flares in our data.

We cannot exclude that the variability of some of these stars are due to being members of binary or multiple systems. One star, #49 (W494) turned out to be a Herbig Ae/Be variable ([Herbst & Shevchenko 1999](#)). Three other stars (#52, #54, #58) are known Orion-type variables ([Samus' et al. 2017](#)). About half of the irregular variables were classified as disk-bearing stars ([Guarcello et al. 2012](#)). They are indicated by ‘db’ in Appendix Table A1. The classification of the identified irregular variables we found is discussed in Sect. 5.4.

5 IDENTIFICATION AND CLASSIFICATION OF PMS STARS

The PMS variable stars, described in Sect. 4.3 and 4.4, can be easily classified on the basis of their infrared excess and the properties of the $H\alpha$ emission line. We therefore had to use external near- and mid-infrared photometry and $riH\alpha$ photometry, which is described in the following subsections.

PMS stars and protostars are subgroups of Young Stellar Objects (YSOs). Based on their spectral index, YSOs have been divided into three main classes, I, II, and III ([Lada 1987](#)). This index is defined as the slope of the spectral energy distribution:

$$\alpha = \frac{d \log(\lambda F_{\lambda})}{d \log \lambda}, \quad (11)$$

where λ is in the range between 1 and 20 μm . Later, [Andre](#)

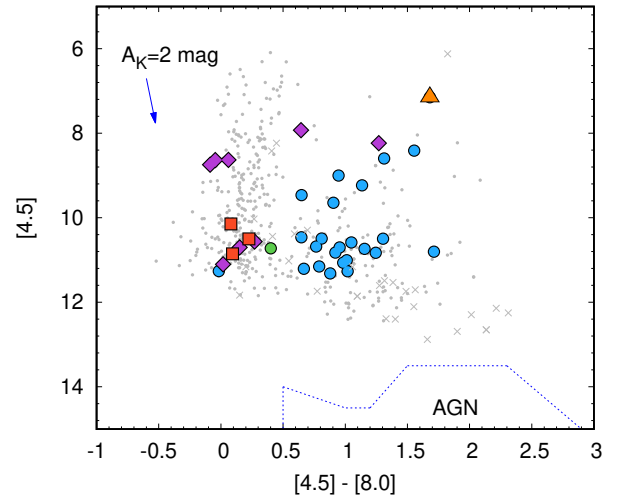


Figure 20. IRAC colour-magnitude diagram. Symbols indicate variable stars found in this study: pulsating stars (red squares), eclipsing stars (pink diamonds), other periodic variables (green circles), H α Be star (orange triangle), and the remaining variables (blue circles). The arrow shows the reddening vector ([Flaherty et al. 2007](#)).

[et al. \(1993\)](#) discovered an extremely young object with a strong emission in the submillimeter domain. Such sources, called Class 0, are not detectable at $\lambda < 10 \mu\text{m}$. Based on the α determinations in the range between 2.2 and 10 μm , [Greene et al. \(1994\)](#) proposed a fifth class, called the ‘flat spectrum’ with α between -0.3 and 0.3 . Objects with $\alpha > 0.3$ were classified as Class I, with $-1.6 < \alpha < -0.3$ as Class II, and with $\alpha < -1.6$ as Class III.

[Lada et al. \(2006\)](#) noted that objects with thick disks have a spectral index of $\alpha > -1.80$, and objects with ‘anemic disks’ (transition disk objects, objects with thin disks) have $-2.56 < \alpha < -1.8$, and objects without disks have $\alpha < -2.56$. Following these authors, the spectral indices α of our variables were calculated for λ between 3.6 and 8 μm using the *Spitzer* photometry described in Sect. 5.1. They are given in Table A1. These indices were useful for classification of pre-main sequence objects, described in Sect. 5.4.

5.1 *Spitzer* and 2MASS photometry

Mid-infrared photometry is very useful for understanding YSOs. Here, we used *Spitzer* photometry taken from the Galactic Legacy Infrared Mid-Plane Survey Extraordinaire (GLIMPSE) catalogue ([Spitzer Science 2009](#)) described by [Benjamin et al. \(2003\)](#). This four-band ([3.6], [4.5], [5.8] and [8.0] μm) photometry was used by [Indebetouw et al. \(2007\)](#), who found a large set of YSOs in the region of NGC 6611. The data from *Spitzer* were also analyzed by [Guarcello et al. \(2009\)](#). Using [3.6]–[4.5] vs. [5.8]–[8.0] colour-colour diagram and reddening-free colour indices, these authors published a catalogue of 474 candidates for pre-main sequence stars with disks and 790 without disks.

To identify YSOs, we used the method described in Appendix A of [Gutermuth et al. \(2009\)](#). Applying an offset of $1''$ between our and *Spitzer* positions, we found about 3000 counterparts in the GLIMPSE catalogue. Only 573 of these have photometry in all four bands. First, we applied the colour and

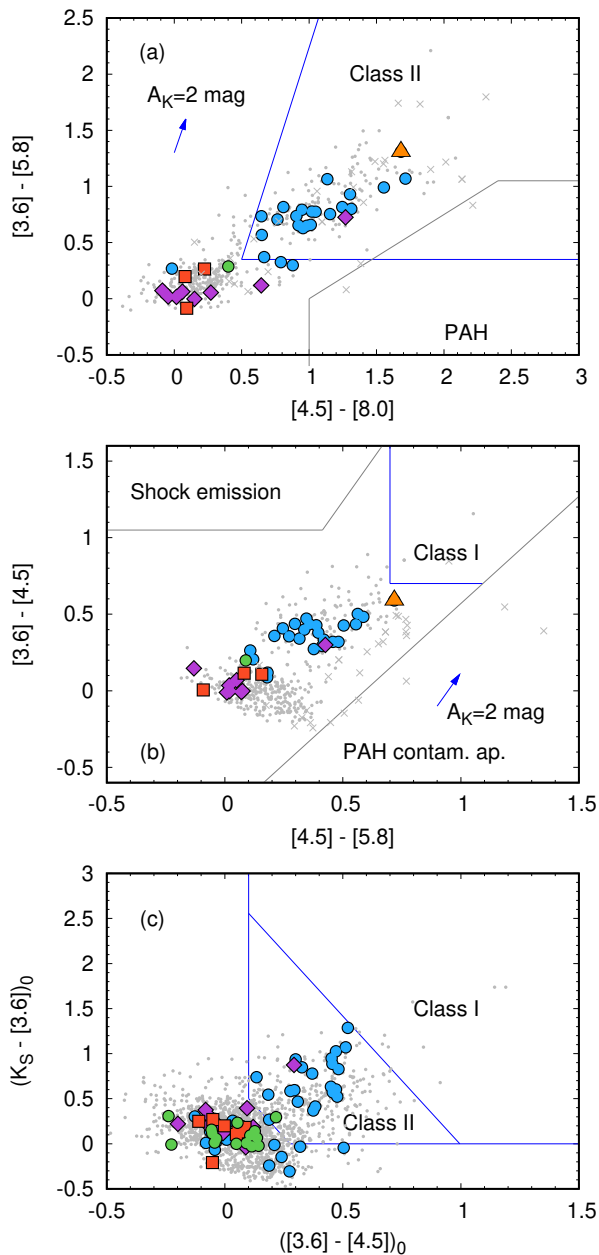


Figure 21. IRAC colour-colour diagrams. The symbols are the same as in Fig. 20.

magnitude criteria of [Gutermuth et al. \(2009\)](#). These allow us to identify extragalactic sources that may be misclassified as YSOs. According to these criteria, two objects appear to be galaxies with bright polycyclic aromatic hydrocarbon (PAH) emission, and 29 sources have aperture photometry contaminated by PAH emission. These objects are marked with crosses in Figs. 20 and 21. We did not find any AGN (active galactic nucleus) or shock emission knots. We extracted Class II objects from the remaining sources, using the colour $[4.5] - [8.0]$ and $[3.6] - [5.8]$ constraints drawn in Fig. 21a. If some of these objects had additional colours $[4.5] - [5.8]$ and $[3.6] - [4.5]$ greater than 0.7, we classified them as Class I objects (Fig. 21b). Among the objects that lack photometry in $[5.8]$ or $[8.0]$ μm but have good-quality 2MASS photom-

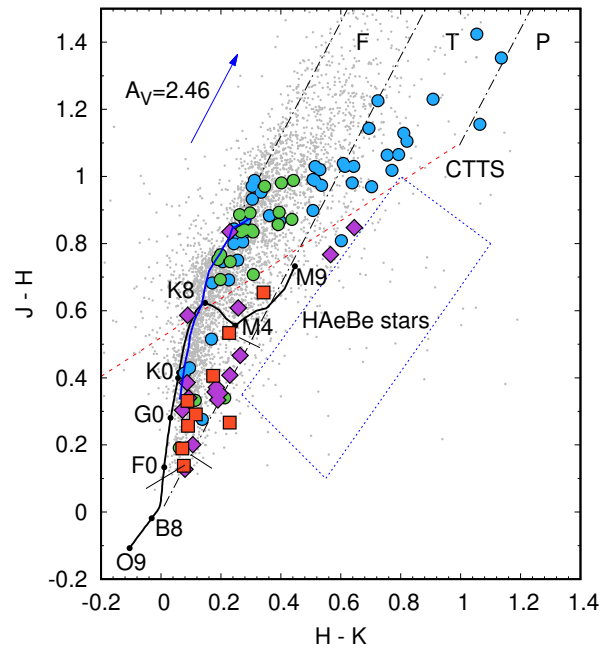


Figure 22. JHK UKIDSS colour-colour diagram for the observed field. The symbols are the same as in Fig. 2. The dashed line is the position of CTTSs ([Meyer et al. 1997](#)). The solid black line is the ZAMS ([Pecaut & Mamajek 2013](#)), and the solid blue line is late-type giants branch ([Bessell & Brett 1988](#)). The arrow shows the reddening vector for $A_V = 2.6$ mag ([Rieke & Lebofsky 1985](#)). The dot-and-dash lines are parallel to the reddening vector, and divided objects into three categories ‘F’, ‘T’, and ‘P’ (see Sect. 5.2). The area delimited by the dotted blue line is the area of dereddened colours for H A e Be stars ([Hernández et al. 2005](#)).

etry, we additionally found several YSOs using dereddened $[3.6] - [4.5]$ and $K_S - [3.6]$ colours (Fig. 21c).

None of the variables we found appears to be Class I object. Out of the 165 objects included in Class II, 20 stars are irregular variables and one is an eclipsing binary (star #11). Most of these stars [Guarcello et al. \(2009\)](#) are found to have an infrared excess and classified as candidates for objects with a disk. Only two objects, star #71 and #74, are classified as being diskless.

5.2 UKIDSS photometry

CTTSs can be easily recognized by their near-infrared excess. JHK photometry was retrieved from the United Kingdom Infrared DeepSky Survey (UKIDSS), carried out with the United Kingdom Infrared Telescope (UKIRT) Wide-Field Camera ([Casali et al. 2007](#)). For almost all the observed objects, we found counterparts in the UKIDSS-DR6 catalogue ([Lucas et al. 2008](#)) within a search radius of $1''$. The JHK data were converted to 2MASS photometry using the transformation relations of [Hewett et al. \(2006\)](#). For objects flagged as ‘close to saturated’ in the UKIDSS-DR6 catalogue, we used magnitudes taken from the 2MASS All-Sky Catalog of Point Sources ([Cutri et al. 2003](#)). The $(J - H)$ vs. $(H - K)$ colour-colour diagram is shown in Fig. 22. The dashed red line indicates the intrinsic locus of CTTSs determined by [Meyer et al. \(1997\)](#). As this line was defined in the CIT (California Institute of Technology) system, the 2MASS magnitudes

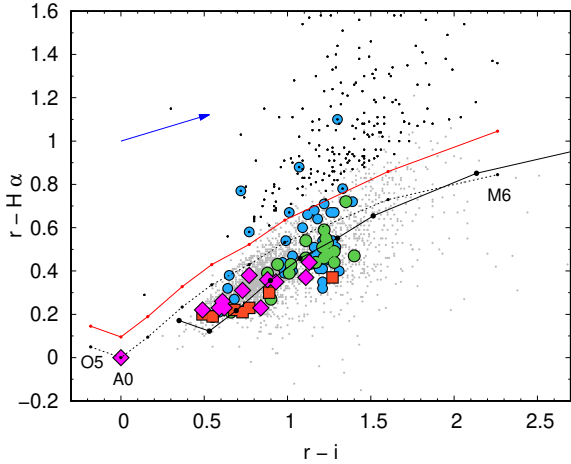


Figure 23. VPHAS $(r - H\alpha)$ vs. $(r - i)$ colour-colour diagram for the observed field. Symbols denote variable stars found in this paper: pulsating (red squares), eclipsing (pink diamonds), HAeBe (orange triangles), other periodic (green circles) and irregular (blue circles).

were transformed to this system using the relations described by Carpenter (2001).

Following Sugitani et al. (2002), we drew three lines parallel to the reddening vector: from the tip of the giant branch (left line), from the base (spectral type A0) of the MS stars (middle line), and from the tip of the intrinsic position of CTTS locus (right line). Objects located between the left and middle lines (‘F’ region) are either field stars (main-sequence or giants) or Class III/Class II sources with small near-infrared (NIR) excesses. Sources lying between the middle and right line (‘T’ region) are mainly CTTSs (Class II sources) with large NIR excesses or Herbig Ae/Be stars with small NIR excess. Sources lying redwards of the ‘T’ region are most likely Class I objects (protostars) or Herbig Ae/Be stars. The blue rectangle denotes the typical dereddened $(J - H)$ and $(H - K)$ colours for HAeBe stars, as defined by Hernández et al. (2005). None of our variables fell into this area. The only HAeBe variable star in our data is flagged as saturated in the UKIDSS data. The other known HAeBe star (W235) is not variable in our data and its UKIDSS photometry is flagged as saturated. Out of 50 stars falling into the HAeBe area, only 9 have a membership probability greater than 50%. They are all non-variable or constant in our data.

5.3 VPHAS photometry

A common feature of CTTSs is an equivalent width of the $H\alpha$ emission line greater than 10 \AA . The intensity of the $H\alpha$ line can be measured by the colour index $(r - H\alpha)$ (Drew et al. 2005). Therefore, we used the $riH\alpha$ photometry obtained during the VST Photometric $H\alpha$ Survey (VPHAS; Drew et al. 2014). We found counterparts in the search radius of $1''$ for about 5300 observed stars. The $(r - H\alpha)$ vs. $(r - i)$ colour-colour diagram for the observed field is shown in Fig. 23. The black dashed line shows the position of the MS stars. The black continuous line is the same position shifted according to the reddening vector for $A_V = 2.6 \text{ mag}$.

The equivalent width ($EW_{H\alpha}$) of each star was calculated

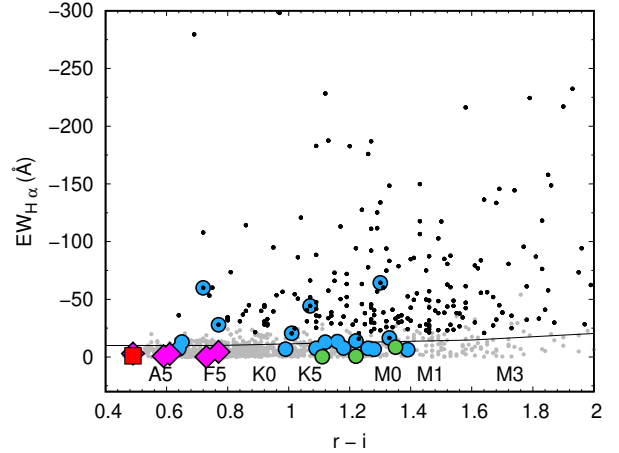


Figure 24. Equivalent width $EW_{H\alpha}$ vs. $(r - i)$ colour for the observed field. The corresponding spectral types are labelled. The colour symbols are the same as in Fig. 23. The black dots represent stars with emission in $H\alpha$ (Sect. 5.3).

by means of the code⁵ of Kalari (2019). Following De Marchi et al. (2010), the author defined $EW_{H\alpha}$ as:

$$EW_{H\alpha} = W \times [1 - 10^{0.4 \times (r - H\alpha)_{\text{excess}}}], \quad (12)$$

where W is the rectangular width of the $H\alpha$ filter and $(r - H\alpha)_{\text{excess}} = (r - H\alpha)_{\text{observed}} - (r - H\alpha)_{\text{model}}$ is the colour excess caused by $H\alpha$ emission (Kalari et al. 2015). To select a CTTSs candidate from the photometric $H\alpha$ emission, we used the same selection threshold as Barentsen et al. (2011). For early-type stars, this threshold (red line in Fig. 23) is the same as a line for $EW_{H\alpha} = 10 \text{ \AA}$, while for stars later than M0, the empirical threshold from Barrado y Navascués & Martín (2003) was adopted. In total, we found 220 stars above the selection threshold, and about half of them are cluster members with a probability greater than 50%. Six of stars are variable. We cannot rule out that some stars may show emission in the $H\alpha$ line but were in quiescent phase of accretion (transitional objects) or the emission was not detected due to intrinsic variability or extinction. The $EW_{H\alpha}$ for the observed stars is shown in Fig. 24.

5.4 Classification of PMS stars

The periodic and irregular variable stars, described in Sect. 4.3 and 4.4 are mainly PMS stars (HAeBe or TTSs). Based on the position in the colour-magnitude and colour-colour diagrams and the spectral index α , we have classified 54 of them. The best candidates for CTTSs are five variables (#52, #56, #85, #86, and #88) with an emission in $H\alpha$ (Sect. 5.3). They all have a strong near-infrared excess and lie in the ‘T’ region in the $(J - H)$ vs. $(H - K)$ colour-colour diagram (Fig. 22). Due to the strong mid-infrared excesses, we classified them as Class II stars with a spectral index of $\alpha > -1.8$. The membership probabilities indicate that one of the CTTSs candidates, star #85, is not a cluster member. Good candidates for CTTSs were 19 variables with near- and

⁵ <https://github.com/astroquackers/HaEW>

mid-infrared excess and $\alpha > -1.8$, but a photometric emission in $H\alpha$ line was not detected. These stars are marked as CTTS* in Table A1. Fifteen were classified as disk-bearing stars (Guarcello et al. 2012).

The stars with a near-infrared excess (lying above CTTS line in the $(J - H)$ vs. $(H - K)$ colour-colour diagram in Fig. 22) and with a spectral index of $\alpha < -1.8$ (or without α), we classified as WTTS. Seventeen are periodic variables, and 13 stars are irregular variables. Most of these stars were classified as disk-less stars (Guarcello et al. 2012).

The ratio of WTTS to CTTS stars counts is equal to 1.25, which is much higher than in case of the cluster of similar age, i.e., NGC 2244 (Michalska 2019) that has a ratio of 0.7. This difference may be due to a less active star-forming process in NGC 6611 than in NGC 2244.

6 SUMMARY AND CONCLUSIONS

In this paper we present the results of a search for variable stars in the young open cluster, NGC 6611. Using combined data collected with three telescopes, we identified 95 variable stars. For 61 variables, the membership probability calculated from the Gaia proper motions is greater than 80%. Among 49 irregular variables, we found 24 CTTS and 13 WTTS candidates. It would be worthwhile to analyze the spectral energy distributions for these stars in the future to determine their stellar properties and of their disks, if they exist. An especially interesting issue worth exploring is if the variability of non-periodic WTTS stars are caused by short-lived irregular spots or by weak accretion from the surrounding thin disk. Out of the 21 periodic variables, we found 17 other WTTS candidates. The large ratio of WTTS to CTTS stars suggests that the star-forming process is not very active in NGC 6611. As for NGC 2244 (Michalska 2019), we found no correlation between period of variability with mass or age. However, our sample is too small for this conclusion to be definitive. More precise observations of NGC 6611 need to be carried out to find more periodic variables. The new data would be also used for the calculation of the standard magnitudes and colours of the stars. This future work would allow us to determine mass-period, age-period and amplitude-period relations, if they exist.

We detected seventeen eclipsing binaries in our field of view. Only two of them were previously known eclipsing binaries, and four other binary stars were newly identified as variables. Eight other variables appear to be δ Scuti pulsating stars. Three are probably cluster members, which means they are pre-main sequence pulsators.

DATA AVAILABILITY

The data underlying this article will be shared on reasonable request to the corresponding author.

APPENDIX A:

In this section we present the coordinates, photometric data and some characteristics of variable stars. In Table A1 the individual columns are:

(1) identification number;

- (2) and (3) right ascension and declination (J2000);
- (4)–(6) average magnitudes and colours (see Sect. 2.2);
- (7)–(8) colours calculated from photometry carried out with 0.9-m CTIO telescope;
- (9) classification taken from Guarcello et al. (2009):
 - A – the source has an infrared excesses and is a candidate for having a circumstellar disk:
 - A01 – member with a circumstellar disk classified based on its position in the IRAC colour-colour diagram;
 - A10 – infrared excesses are detected only by Q indices ($Q_{V-IJ[sp]} = (V - I) - (J - [sp]) \times E_{V-I}/E_{J-[sp]}$ where $[sp]$ is the magnitude in a given IRAC band);
 - A11 – both diagnostics (IRAC colour-colour diagram and Q indices) detect emission from the disk;
 - B – the star is an X-ray source without infrared excesses, candidate for a member without a disk;
 - C – the star is an X-ray source without infrared excesses which optical colours are consistent with foreground main-sequence stars;
- (10) Classification based on optical/infrared properties taken from Guarcello et al. (2012):
 - db – disk-bearing member;
 - dl – disk-less member;
- (11) $EW_{H\alpha}$ – equivalent width of $H\alpha$ emission computed by the code of Kalari (2019) (Sect. 5.3);
- (12) Classification based on *Spitzer* photometry (Sect. 5.1):
 - II – Class II objects (II* denote object with photometric uncertainty larger than required in method of Gutermuth et al. (2009) used to this classification);
 - III – field stars and/or diskless YSOs (Class III);
- (13) Area in $(J - H) - (H - K)$ colour-colour diagram in Fig. 22;
- (14) Spectral index $\alpha = d \log(\lambda F_\lambda) / d \log(\lambda)$ calculated from the slope of the linear fit to the fluxes between the K band and the IRAC [8] μm band (Lada et al. 2006);
- (15) Membership probability determined in Sect. 3;
- (16) Variability type:
 - ECL – eclipsing binary;
 - ELL – ellipsoidal star;
 - CTTS – the best candidates for CTTSs: Class II stars with photometric $EW_{H\alpha} < -10 \text{ \AA}$ lying above CTTS line in $(J - H) - (H - K)$ colour-colour diagram (Fig. 22);
 - CTTS* – candidates for CTTSs lying above CTTS line (Class III stars with photometric $EW_{H\alpha} < -10 \text{ \AA}$ and Class II objects having spectral index $\alpha > -1.8$ with photometric $EW_{H\alpha} > -10 \text{ \AA}$) or without $EW_{H\alpha}$;
 - WTTS – candidates for WTTSs: objects lying above the CTTS line for which no spectral index α was calculated or $\alpha < -1.8$;
 - PER – periodic variable which was not classified as WTTS;
 - IRR – irregular variable which was not classified as CTTS;
- (17) object type taken from Simbad database;
- (18) spectral type;
- (19) WEBDA² ID number found within a search radius of 1'';
- (20) Other name from GCVS, or HD catalogue.

Description of Table A2:

- (1) ID number;
- (2) Gaia DR2 ID;
- (3)–(5) Gaia DR2 magnitudes and colours;
- (6)–(8) 2MASS photometry;
- (9)–(11) UKIDSS photometry;
- (12)–(15) IRAC photometry;
- (16)–(18) VPHAS photometry.

Table A1. $UBVI_C$ photometry and coordinates of variable stars found in NGC 6611 along with some important information about these stars.

Star	R.Asc. (2000.0)	Dec. (2000.0)	V mag	V-I _C mag	B-V mag	B-V mag	U-B mag	G09	G12	EW _{Hα}	Cl.	NIR reg. (13)	α (14)	Prob. [%] (15)	Var. type (16)	Notes (17)	Spectral type (18)	Webda ID (19)	Other name (20)
(1)	(2)	(3)	(4)	(5)	(6)	(7)	(8)	(9)	(10)	(11)	(12)	(13)	(14)	(15)	(16)	(17)	(18)	(19)	(20)
Eclipsing binaries																			
1	18:18:45.85	-13:46:30.89	9.790	0.909	0.684	0.587	-0.428	B	dl	–	III	–	-2.05	60.9	ECL	YSO	B0.5V+B0.5V	314	BD -13 ^o 4929
2	18:18:42.78	-13:46:50.97	10.094	0.692	0.520	0.435	-0.615	B	dl	–	III	–	-2.89	97.3	ECL	Be*	O9.5V	280	BD -13 ^o 4928
3	18:18:49.38	-13:46:50.04	11.792	1.331	0.854	0.841	0.233	–	–	–	III	–	-2.92	18.4	ECL	Star	B1V	343	ALS 15387
4	18:19:00.43	-13:42:41.02	12.603	1.341	0.925	0.811	-0.019	B	–	–	–	–	-2.17	94.5	ELL	YSO	B1.5V	444	ALS 15393
5	18:18:33.72	-13:40:58.86	13.019	2.088	1.438	–	–	B	dl	–	–	–	-2.77	20.8	ECL	YSO	B0V	188	ALS 15355
6	18:18:38.40	-13:47:09.06	12.794	0.958	0.693	0.604	-0.229	B	dl	-2.6	III	–	-2.50	95.5	ECL	Em*	B1.5Ve	227	ALS 15364
7	18:18:21.78	-13:55:05.15	12.821	0.962	0.876	0.777	0.255	–	–	-3.0	III	–	-2.69	0.0	ECL	Star	–	94	–
8	18:19:04.71	-13:44:44.56	12.846	0.737	0.575	0.480	-0.211	–	–	-1.0	–	–	-2.72*	96.4	ELL	Em*	B3Ve	472	–
9	18:18:46.13	-13:54:37.18	13.483	0.974	0.879	0.761	0.228	B	dl	-0.7	–	–	-2.95*	0.1	ECL	YSO	B+G+emis.	310	ALS 15383
10	18:18:41.54	-13:48:40.41	13.792	0.978	0.742	0.649	0.035	–	–	–	III	–	-2.71	81.6	ECL	Em*	B7	262	ALS 15370
11	18:18:41.58	-13:46:30.92	14.735	1.832	1.415	1.389	-0.611	A11	–	–	II	–	-1.03	96.5	ECL	Em*	G:	266	–
12	18:18:34.63	-13:39:48.99	15.495	3.160	2.135	–	–	–	–	–	–	–	–	90.0	ECL	YSOC	–	2303	–
13	18:18:41.16	-13:48:21.10	15.265	1.165	1.116	1.018	0.363	–	–	-0.1	–	–	-1.75*	0.0	ECL	Star	–	258	–
14	18:18:32.69	-13:54:47.81	16.813	1.369	1.289	–	–	–	–	-4.5	–	–	–	0.0	ECL	–	–	15536	–
15	18:18:41.43	-13:47:08.33	17.599	2.243	1.654	–	–	B	dl	–	–	–	-1.45*	96.9	ECL	YSO	–	16215	–
16	18:18:33.37	-13:46:56.44	17.794	1.498	1.286	–	–	C	dl	–	–	–	–	0.0	ELL	YSO	–	17759	–
17	18:18:39.01	-13:42:30.79	18.096	1.656	1.385	–	–	–	–	–	–	F	–	0.0	ECL	–	–	6338	–
Pulsating stars																			
18	18:18:27.79	-13:55:04.86	12.845	0.924	0.881	0.768	0.450	–	–	–	III	–	-2.76	0.0	DSCT	Star	F0III/V	135	–
19	18:18:53.27	-13:46:07.18	13.363	1.360	1.067	0.951	0.625	B	dl	–	III	–	-2.62	94.8	DSCT	Em*	F2e	374	–
20	18:18:37.64	-13:45:13.22	14.461	1.584	1.162	1.040	0.683	B	dl	–	III	–	-2.45	97.0	DSCT	Em*	B8Ve	221	–
21	18:18:49.36	-13:39:08.36	14.266	1.053	0.903	–	–	–	–	–	–	–	-2.15*	0.0	DSCT	Star	A7III	347	–
22	18:19:00.93	-13:38:49.07	14.292	0.895	0.793	–	–	–	–	–	–	–	–	0.0	DSCT	YSO	–	451	–
23	18:19:07.43	-13:40:37.93	15.275	2.439	1.653	–	–	–	dl	–	–	–	-2.50*	91.5	DSCT	YSO	–	491	–
24	18:18:42.04	-13:47:14.02	15.431	1.198	1.001	0.890	0.456	A10	–	–	–	–	–	0.0	DSCT	YSOC	–	270	–
25	18:18:59.58	-13:45:39.46	15.474	1.196	0.963	0.849	0.600	–	–	–	–	–	–	93.5	DSCT	Star	–	435	–
Other periodic variables																			
26	18:19:04.82	-13:52:32.36	14.522	0.828	0.761	0.665	0.249	–	–	–	–	–	–	0.0	PER	Star	–	465	–
27	18:18:14.15	-13:43:45.60	15.341	1.139	0.950	–	–	–	–	–	–	–	–	0.0	PER	Star	–	59	–
28	18:18:29.54	-13:42:30.33	15.649	1.645	1.212	1.095	0.580	–	–	–	–	–	–	1.6	PER	Star	–	154	–
29	18:18:47.79	-13:48:15.34	16.217	2.344	1.886	–	–	A10	db	–	–	F	-2.75*	–	WTTS	YSO	–	16091	–
30	18:19:03.16	-13:45:11.23	16.521	2.349	1.867	–	–	B	dl	–	–	F	-2.49*	96.4	WTTS	YSO	–	456	–
31	18:18:39.72	-13:48:41.22	16.444	1.891	1.549	–	–	B	dl	–	–	F	-2.81*	93.9	WTTS	YSO	–	1182	–
32	18:18:36.23	-13:46:19.16	16.724	2.103	1.639	–	–	B	dl	–	–	F	-2.01*	96.7	WTTS	YSO	–	16600	–
33	18:18:45.96	-13:47:52.67	16.895	2.340	1.777	–	–	A10	db	–	III	F	-2.18	96.7	WTTS	YSO	–	16758	–
34	18:18:30.41	-13:51:47.24	16.695	1.910	1.644	–	–	B	dl	–	–	F	-2.06*	96.7	WTTS	YSO	–	15742	–
35	18:18:45.92	-13:55:22.03	16.569	1.815	1.510	–	–	B	dl	–	–	F	–	95.9	PER	YSO	–	15488	–
36	18:18:46.02	-13:50:09.07	17.572	1.979	1.533	–	–	B	dl	–	–	F	–	88.3	WTTS	YSO	–	15877	–
37	18:18:41.86	-13:47:23.07	17.991	2.202	1.385	–	–	B	dl	–	–	F	–	96.5	WTTS	YSO	–	17002	–
38	18:19:01.20	-13:47:19.53	18.172	2.425	1.311	–	–	A10	dl	–	–	F	–	87.8	WTTS	YSO	–	13002	–
39	18:19:07.26	-13:43:47.98	18.519	2.439	–	–	–	B	dl	–	–	F	–	55.9	WTTS	YSO	–	4610	–
40	18:18:41.93	-13:48:59.90	18.486	2.297	1.136	–	–	B	dl	–	–	F	–	96.8	WTTS	Em*	–	17389	–
41	18:18:42.04	-13:53:17.23	18.530	2.280	1.325	–	–	B	dl	-0.3	–	F	–	93.4	WTTS	YSO	–	15644	–
42	18:18:59.26	-13:46:41.88	18.608	2.304	–	–	–	B	dl	–	–	F	–	87.4	WTTS	YSO	–	13088	–
43	18:18:26.05	-13:47:35.88	18.826	2.717	–	–	–	B	dl	–	–	F	–	79.7	WTTS	YSO	–	16165	–
44	18:18:41.81	-13:47:29.21	18.727	2.284	–	–	–	B	db	-0.7	–	F	–	96.3	WTTS	YSO	–	16537	–
45	18:18:30.77	-13:43:46.63	19.193	2.658	–	–	–	B	dl	–	–	F	–	83.2	WTTS	YSO	–	7906	–
46	18:18:58.14	-13:54:32.03	18.933	2.452	–	–	–	B	db	-8.5	–	F	–	11.4	WTTS	YSO	–	13244	–

Table A1 – *continued*

Star	R.Asc. (2000.0)	Dec. (2000.0)	V mag	V-I _C mag	B-V mag	B-V mag	U-B mag	G09	G12	EW _{Hα}	Cl.	NIR reg.	α	Prob. [%]	Var. type	Notes	Spectral type	Webda ID	Other name	
(1)	(2)	(3)	(4)	(5)	(6)	(7)	(8)	(9)	(10)	(11)	(12)	(13)	(14)	(15)	(16)	(17)	(18)	(19)	(20)	
Irregular variables																				
47	18:18:46.61	-13:46:59.89	13.572	0.954	0.725	0.626	0.010	-	dl	-	-	-	-3.73*	96.4	IRR	Em*	B8V:e	322		
48	18:18:59.16	-13:39:55.32	14.204	1.219	1.079	-	-	-	-	-	-	-	-2.41*	0.0	IRR	YSO	-	439		
49	18:19:09.39	-13:50:41.20	13.945	1.027	0.752	0.661	0.237	A01	-	-	II	-	-0.20	95.4	Haebe	Ae*	Be	494	EU Ser	
50	18:18:33.28	-13:54:11.17	14.850	1.354	1.216	1.063	0.595	B	dl	-7.0	-	-	-3.01*	0.0	IRR	YSO	-	172		
51	18:18:39.37	-13:47:11.79	15.863	1.899	1.619	-	-	-	dl	-	-	III	-	-2.73	97.0	IRR	YSO	-	642	
52	18:19:13.82	-13:58:44.86	-	-	-	-	-	A11	-	-60.0	II	P	-0.94	95.5	CTTS	Or*	-	1289	EV Ser	
53	18:18:37.56	-14:01:12.75	-	-	-	-	-	-	-	-13.0	-	-	-	0.0	IRR	-	-	16643		
54	18:18:58.53	-13:48:28.43	16.995	2.241	1.770	-	-	A01	db	-	II	-	-1.71	96.0	IRR	Or*	-	14021	FN Ser	
55	18:18:48.23	-13:49:08.27	16.953	2.272	1.633	-	-	A11	db	-13.3	II	T	-1.27	95.7	CTTS*	Em*	-	16907		
56	18:19:20.89	-13:42:04.14	16.935	-	1.263	-	-	A11	-	-27.8	II	T	-0.54	96.9	CTTS	YSOC	-	546		
57	18:19:20.03	-13:49:12.82	16.723	-	1.480	-	-	A11	db	-	II	-	-1.20	96.0	IRR	YSO	-	12804		
58	18:18:39.83	-13:47:44.40	16.661	2.114	1.868	-	-	B	dl	-7.9	-	-	-	0.0	IRR	Star	-	1767	FM Ser	
59	18:19:24.24	-13:45:47.65	16.922	-	1.598	-	-	-	dl	-	-	F	-	0.0	WTTS	-	-	10134		
60	18:19:06.61	-13:45:36.61	17.073	2.541	1.790	-	-	A10	db	-	-	T	-1.38*	95.8	CTTS*	YSO	-	4394		
61	18:18:49.90	-13:46:59.65	17.422	2.542	1.874	-	-	A11	db	-	II	T	-0.94	97.0	CTTS*	YSO	-	13049		
62	18:19:14.81	-13:46:14.24	17.183	2.310	1.659	-	-	B	dl	-	-	F	-2.48*	5.3	WTTS	YSO	-	13134		
63	18:18:49.84	-13:48:17.42	17.376	2.289	1.804	-	-	B	dl	-	-	F	-2.85*	96.3	WTTS	YSO	-	13831		
64	18:18:39.18	-13:46:04.93	17.517	2.349	1.693	-	-	A10	dl	-	-	F	-2.48*	96.8	WTTS	YSO	-	16587		
65	18:18:59.83	-13:46:10.57	17.462	2.232	1.742	-	-	B	dl	-	-	F	-2.11*	90.7	WTTS	YSO	-	13136		
66	18:18:40.09	-13:46:52.67	17.529	2.294	1.353	-	-	A11	db	-	II	F	-0.84	94.5	CTTS*	YSO	-	18221		
67	18:19:06.19	-13:44:28.59	17.647	2.445	1.583	-	-	A10	db	-	III	F	-1.11	83.8	CTTS*	YSO	-	4534		
68	18:18:52.41	-13:46:58.50	17.718	2.426	1.714	-	-	A11	db	-	II	T	-1.59	89.4	CTTS*	Em*	-	13051		
69	18:18:38.55	-13:51:10.31	17.599	2.054	1.615	-	-	B	dl	-	-	F	-	96.0	WTTS	YSO	-	15777		
70	18:18:52.13	-13:48:10.18	17.459	2.132	1.614	-	-	A11	db	-7.6	II	T	-1.38	96.3	CTTS*	Em*	-	14681		
71	18:19:08.45	-13:47:52.77	18.026	2.459	1.971	-	-	B	dl	-	II	T	-1.12	13.9	CTTS*	YSO	-	12927		
72	18:18:55.24	-13:47:59.55	17.781	2.039	1.625	-	-	B	dl	-	-	F	-	96.7	WTTS	YSO	-	13730		
73	18:18:37.94	-13:51:56.24	18.090	2.584	1.705	-	-	B	dl	-16.5	-	-	-2.77*	73.1	IRR	YSO	-	15731		
74	18:19:00.21	-13:45:39.97	17.706	2.470	1.562	-	-	B	db	-	II	F	-1.35	0.0	CTTS*	YSO	-	4389		
75	18:19:05.67	-13:44:44.59	17.821	2.229	1.454	-	-	A11	dl	-	II	F	-1.36	-	CTTS*	YSOC	-	6049		
76	18:18:38.72	-13:48:54.01	17.834	2.156	1.556	-	-	B	dl	-	-	F	-1.03*	93.2	CTTS*	YSO	-	16012		
77	18:19:05.90	-13:47:51.79	18.116	2.369	1.664	-	-	B	db	-	III	F	-1.73	94.2	CTTS*	YSO	-	12931		
78	18:18:42.71	-13:47:30.24	17.948	2.289	1.322	-	-	B	db	-	-	F	-1.81	93.8	WTTS	YSO	-	16173		
79	18:18:55.31	-13:46:51.72	17.963	2.454	1.454	-	-	A11	db	-7.5	III	F	-1.61	86.0	CTTS*	Em*	-	13563		
80	18:18:40.48	-13:47:18.30	18.113	2.275	1.308	-	-	A01	db	-	II	F	-1.27	96.3	CTTS*	YSO	-	16201		
81	18:18:37.43	-13:46:08.03	18.083	2.678	-	-	-	A11	db	-	II	T	-1.35	90.0	CTTS*	YSO	-	16593		
82	18:18:39.47	-14:00:34.05	17.777	-	1.505	-	-	A11	-	-6.8	II	T	-0.93	96.8	CTTS*	YSOC	-	16674		
83	18:19:11.56	-13:42:38.43	18.512	2.514	-	-	-	A10	db	-	-	F	-2.33*	96.4	WTTS	YSO	-	4725		
84	18:19:06.85	-13:52:40.45	18.344	2.334	1.610	-	-	B	dl	-	-	F	-	96.1	WTTS	YSO	-	12569		
85	18:18:58.61	-13:49:56.84	18.261	2.194	1.183	-	-	A10	db	-20.5	II	T	-1.38	14.4	CTTS	YSO	-	12743		
86	18:18:47.98	-13:48:36.25	18.797	2.675	-	-	-	A11	db	-64.2	II	T	-0.31	95.5	CTTS	Em*	-	16508		
87	18:18:35.56	-13:45:58.16	18.787	2.544	-	-	-	B	dl	-6.6	-	F	-	96.5	WTTS	YSO	-	10178		
88	18:18:30.54	-13:54:46.01	18.602	2.248	-	-	-	A01	db	-44.2	II*	T	-1.23	85.7	CTTS	YSO	-	-		
89	18:18:47.86	-13:50:01.31	18.695	2.327	-	-	-	B	db	-13.9	-	F	-1.26*	0.0	CTTS*	YSO	-	15894		
90	18:18:37.14	-13:45:05.83	18.942	2.557	-	-	-	B	dl	-	-	F	-	96.4	WTTS	YSO	-	7976		
91	18:18:47.91	-13:55:13.93	19.260	2.336	-	-	-	B	db	-12.9	III	T	-1.70	95.3	CTTS*	YSO	-	15501		
92	18:18:38.69	-13:44:57.53	18.858	2.645	-	-	-	A10	db	-6.4	II	T	-1.30	88.2	CTTS*	YSO	-	8062		
93	18:18:32.28	-13:47:02.71	19.516	2.582	-	-	-	B	dl	-	-	-	-	96.1	WTTS	YSO	-	16703		
94	18:18:42.02	-13:48:03.67	-	-	-	-	-	A11	db	-	-	-	-	-	IRR	YSO	-	16119		
95	18:19:16.11	-13:34:57.87	-	-	-	-	-	-	-	-	-	-	-	-	IRR	-	-	5249		

Table A2. Gaia DR2, 2MASS, UKIDSS and Spitzer infrared photometry of variable stars.

Star	Gaia DR2 ID	G	BP	RP	J	H	K _S	J	H	K	[3.6]	[4.5]	[5.8]	[8.0]	r	i	H _α
(1)	(2)	mag (3)	mag (4)	mag (5)	mag (6)	mag (7)	mag (8)	mag (9)	mag (10)	mag (11)	mag (12)	mag (13)	mag (14)	mag (15)	mag (16)	mag (17)	mag (18)
Eclipsing binaries																	
1	4146600781797073920	9.587	9.587	10.012	8.248	8.077	7.937	–	–	11.206	7.997	7.928	7.878	7.283	–	–	–
2	4146600678717290624	9.922	9.922	10.219	8.961	8.869	8.755	11.346	12.087	–	8.631	8.633	8.612	8.678	–	–	–
3	4146600708779213312	11.304	11.304	11.920	9.476	9.119	8.900	10.436	10.674	9.691	8.742	8.744	8.669	8.831	–	–	–
4	4152606172568933504	12.241	12.241	12.847	10.300	9.958	9.744	10.930	11.177	10.236	–	–	–	–	–	–	–
5	4146614319533501440	12.271	12.271	13.328	9.534	9.074	8.776	10.622	11.615	9.692	8.624	8.631	8.561	8.571	11.93	12.30	11.19
6	4146600640059737088	12.526	12.526	12.945	11.048	10.725	10.598	11.175	11.181	10.643	10.597	10.562	10.543	10.291	12.14	12.40	11.79
7	4146592191861866112	12.647	12.647	13.105	11.231	10.948	10.842	11.377	11.678	–	10.692	10.703	10.694	10.553	12.23	12.45	11.96
8	4146601022314634368	12.729	12.729	13.022	11.610	11.507	11.397	11.623	11.678	11.426	–	–	–	–	12.42	12.62	12.13
9	4146594219086377728	13.326	13.326	13.752	11.907	11.569	11.339	11.853	11.695	11.492	–	–	–	–	12.91	13.14	12.55
10	4146598887718489984	13.563	13.563	13.984	12.062	11.746	11.522	11.982	11.827	11.653	11.249	11.102	11.233	11.085	13.20	13.43	12.81
11	4146600678717298304	13.677	13.677	14.535	11.160	10.286	9.607	11.228	11.523	10.113	8.532	8.233	7.807	6.963	13.28	13.63	12.70
12	4146614353893249024	13.904	13.904	15.687	10.043	9.256	8.656	10.558	11.256	9.622	–	–	–	–	–	–	–
13	4146599098169306624	14.925	14.925	15.477	13.168	12.738	12.613	13.076	12.729	12.588	–	–	–	–	14.67	14.98	14.25
14	4146597272809633152	16.560	16.560	16.831	–	–	–	14.528	14.169	13.862	–	–	–	–	16.08	16.46	15.69
15	4146600640066272512	16.722	16.722	17.289	13.739	12.809	12.481	13.702	12.910	12.603	–	–	–	–	16.39	16.83	15.70
16	4146610982347466624	17.275	17.275	17.498	–	–	–	15.151	14.592	14.251	–	–	–	–	16.86	17.09	16.25
17	4146613284443719552	17.628	17.628	18.370	15.186	14.419	14.226	15.193	14.643	14.499	–	–	–	–	16.93	17.29	16.41
Pulsating stars																	
18	4146591470307346944	12.690	12.690	13.138	11.316	11.084	10.960	11.452	11.738	–	10.859	10.853	10.944	10.760	12.29	12.48	11.93
19	4146600541278311680	12.968	12.968	13.626	10.919	10.525	10.317	11.119	11.149	10.433	10.260	10.145	10.063	10.065	12.63	12.86	12.09
20	4146612498467320064	13.955	13.955	14.708	11.588	11.055	10.794	11.547	11.433	10.825	10.608	10.500	10.343	10.275	13.59	13.89	13.00
21	4152619061778260992	14.052	14.052	14.536	12.512	12.199	12.077	12.435	12.250	12.099	–	–	–	–	–	–	–
22	4152618374583531008	14.124	14.124	14.545	12.762	12.472	12.380	12.701	12.551	12.429	–	–	–	–	–	–	–
23	4152618099705619712	14.262	14.262	15.558	11.048	10.384	10.008	11.231	11.231	10.342	–	–	–	–	14.07	14.44	13.17
24	4146600644357549440	15.105	15.105	15.591	13.310	12.916	12.208	13.262	13.046	12.740	–	–	–	–	14.75	14.97	14.29
25	4146600953595160704	15.162	15.162	15.665	–	–	–	13.281	13.032	12.857	–	–	–	–	14.86	15.07	14.34
Other periodic variables																	
26	4146596177591442688	14.385	14.385	14.750	13.097	12.932	12.824	13.045	12.893	12.782	–	–	–	–	14.04	14.23	13.68
27	4146612326668690816	15.073	15.073	15.604	13.338	12.973	12.785	13.287	12.995	12.822	–	–	–	–	14.71	14.92	14.26
28	4146613701058707200	15.077	15.077	15.878	12.799	12.476	12.229	12.729	12.435	12.209	–	–	–	–	14.79	15.06	14.16
29	4146600369479609344	15.151	15.151	16.179	12.091	11.167	10.739	12.025	11.371	10.853	–	–	–	–	14.71	15.22	14.01
30	4146600983663759104	15.557	15.557	16.575	12.462	11.540	11.209	12.282	11.628	11.158	–	–	–	–	15.26	15.72	14.50
31	4146599063809568000	15.718	15.718	16.434	13.013	12.291	11.949	13.103	12.450	12.177	–	–	–	–	15.22	15.65	14.63
32	4146612459816239232	15.845	15.845	16.687	13.016	12.245	12.021	13.151	12.349	11.960	–	–	–	–	15.40	15.86	14.75
33	4146600365188397568	15.872	15.872	16.708	12.735	11.851	11.426	12.625	11.816	11.407	10.922	10.724	10.635	10.323	15.48	15.96	14.72
34	4146598303597678336	15.905	15.905	16.793	13.498	12.712	12.479	13.348	12.734	–	–	–	–	–	15.40	15.79	14.78
35	4146594180429043200	15.942	15.942	16.737	–	–	–	13.325	12.748	12.449	–	–	–	–	15.48	15.87	14.99
36	4146598028725056128	16.799	16.799	17.070	14.231	13.382	13.132	14.086	13.384	13.075	–	–	–	–	16.40	16.83	15.89
37	4146600644357547648	17.068	17.068	17.384	13.608	12.636	12.178	13.875	13.225	12.954	–	–	–	–	16.64	17.08	15.91
38	4146600094601679360	17.182	17.182	17.537	13.978	12.945	12.440	13.862	13.021	12.676	–	–	–	–	16.87	17.40	16.16
39	4152605897695277568	17.389	17.389	17.998	14.180	13.255	12.942	14.074	13.280	12.915	–	–	–	–	17.11	17.55	16.27
40	4146598887718492416	17.473	17.473	17.765	14.269	13.398	13.087	14.236	13.450	13.053	–	–	–	–	17.26	17.75	16.47
41	4146597238451051648	17.490	17.490	17.464	14.327	13.440	13.141	14.250	13.459	13.066	–	–	–	–	17.10	17.64	16.53
42	4146600850510993664	17.593	17.593	17.870	14.593	13.681	13.431	14.403	13.614	13.263	–	–	–	–	17.25	17.80	16.57
43	4146610849199880960	17.640	17.640	18.441	–	–	–	13.927	13.007	12.564	–	–	–	–	17.25	17.72	16.32
44	4146600575638068992	17.654	17.654	17.640	–	–	–	14.514	13.588	13.080	–	–	–	–	17.26	17.85	16.63
45	4146613524968091392	17.959	17.959	18.139	14.175	13.245	12.723	14.202	13.271	12.717	–	–	–	–	–	–	–
46	4146594352231975296	18.133	18.133	17.464	–	–	–	14.561	13.747	13.198	–	–	–	–	17.26	17.98	16.63

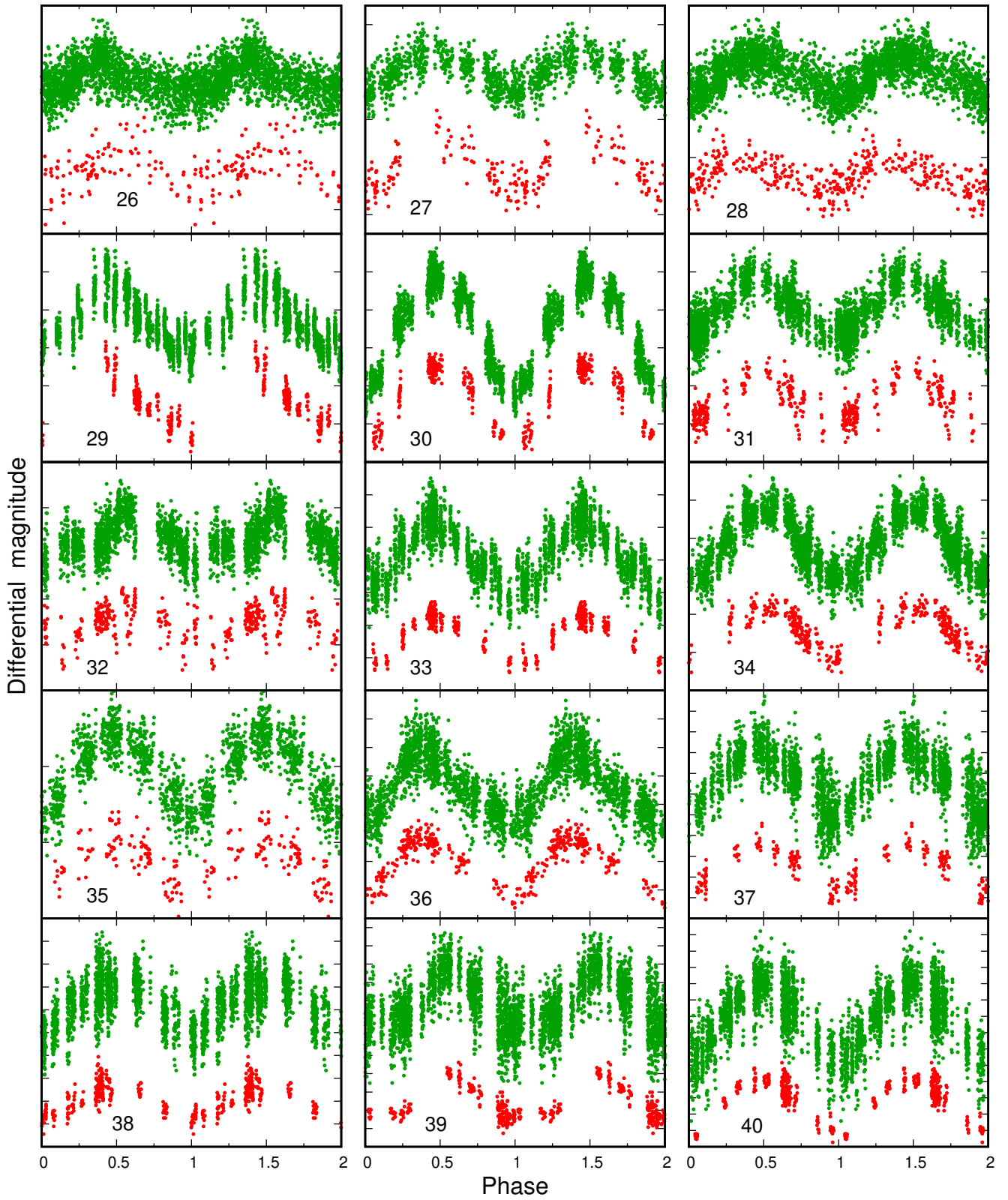
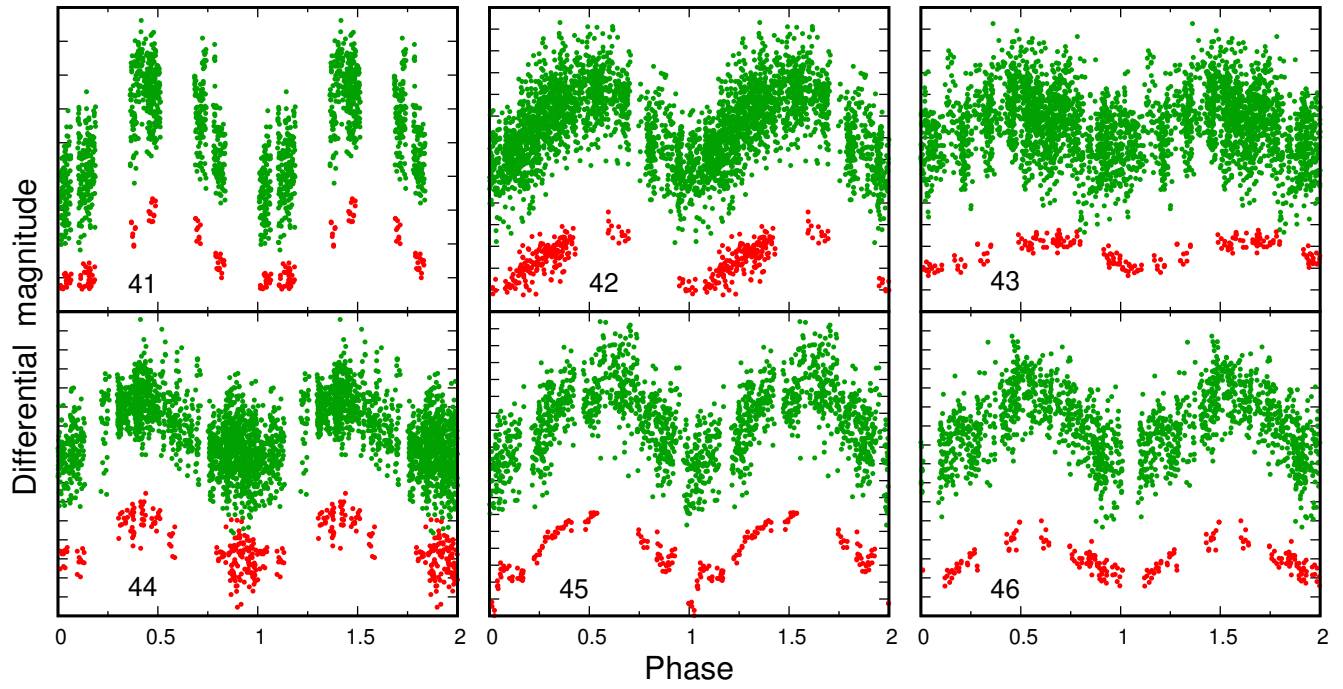


Figure B1. Phase diagrams of B (blue), V (green) and I (red) observations of other periodic variables found in the observed field of NGC 6611 (Sect. 4.3). Star numbers are given in the panels. The ordinate ticks are separated by 0.1 mag.

Figure B1 – *continued*

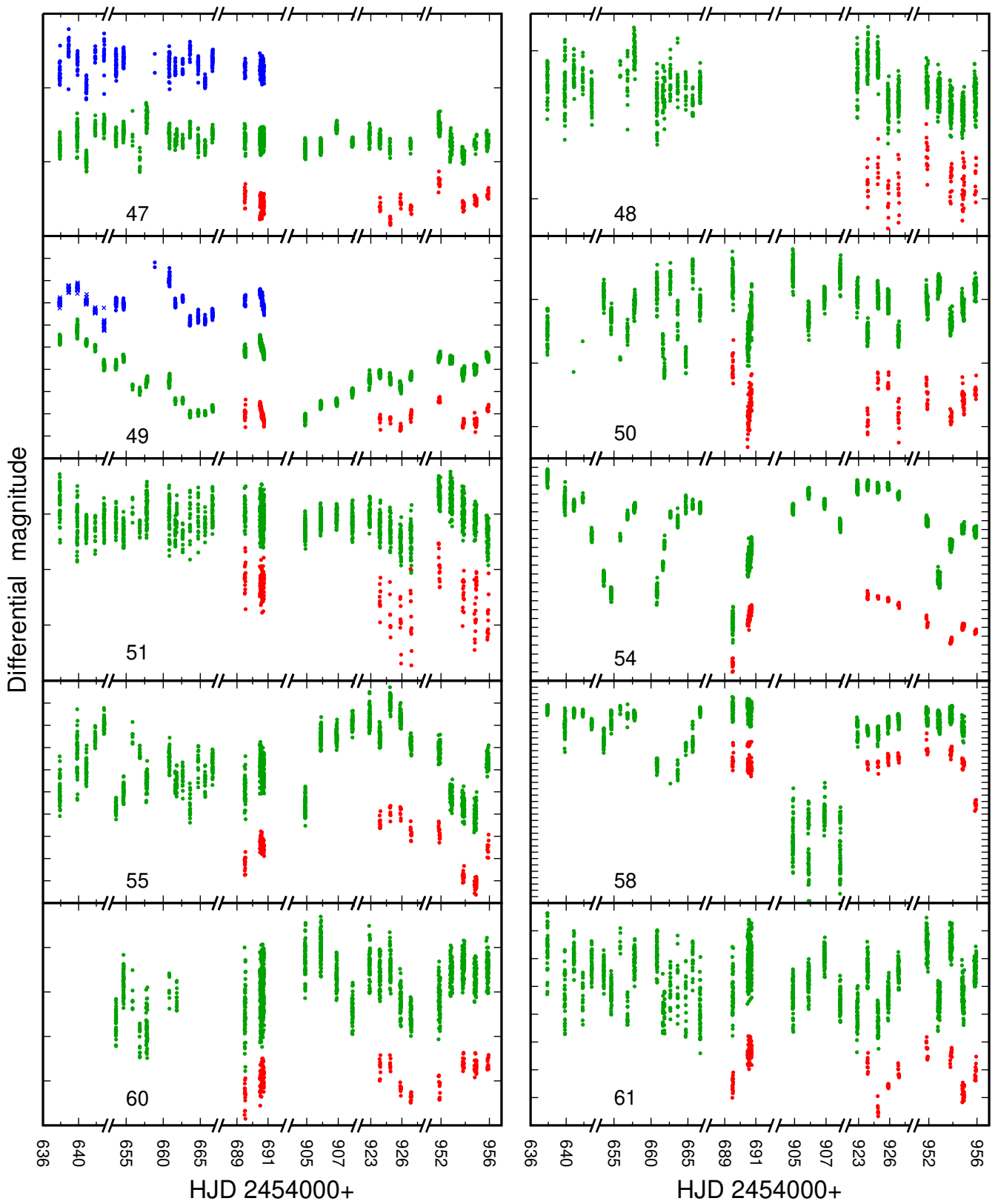


Figure B2. Light curves of irregular variables found in the observed field of NGC6611 (Sect. 4.4) in *B* (blue), *V* (green) and *I* (red) passbands. Star numbers are given in the numbers. The ordinate ticks are separated by 0.1 mag.

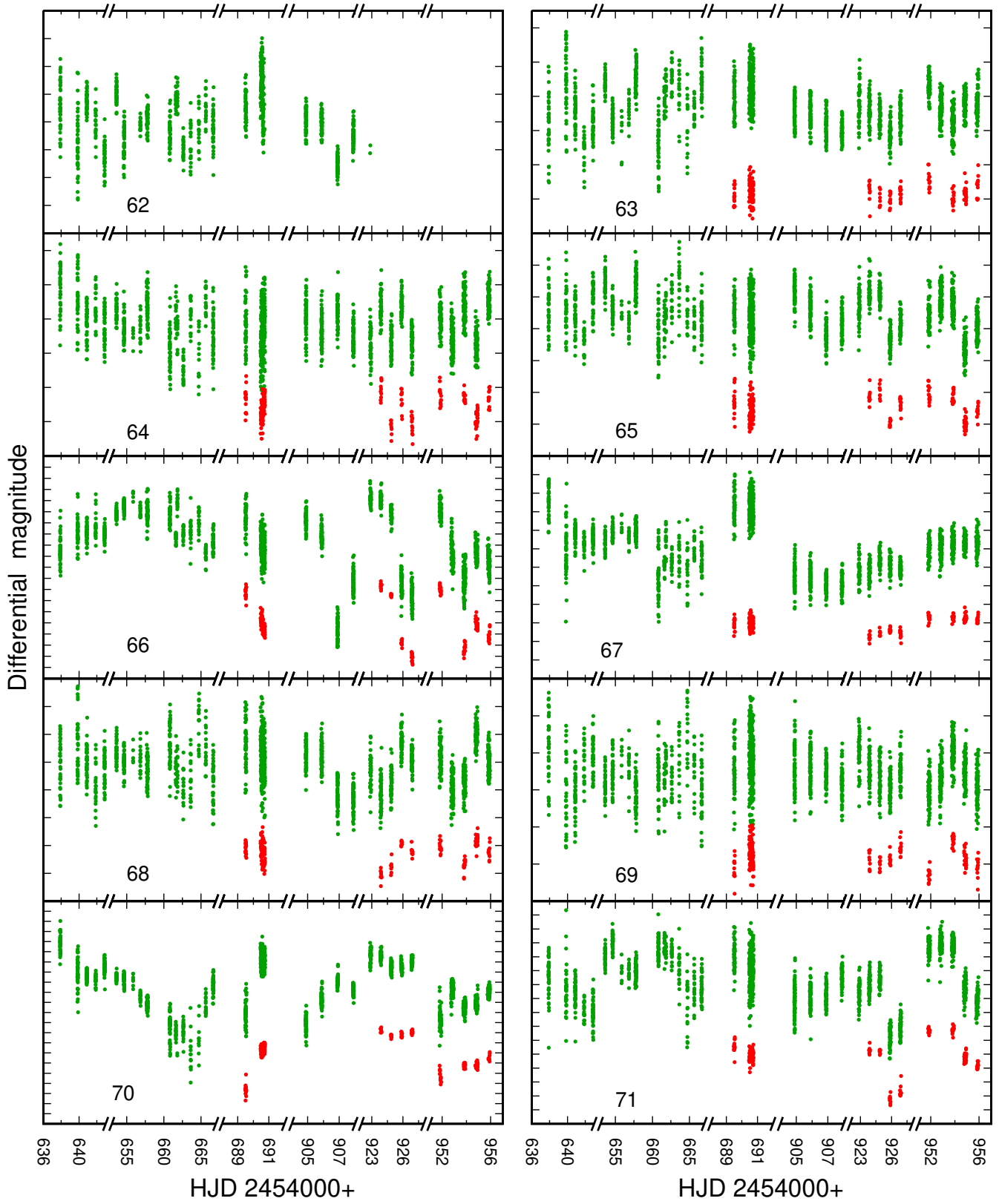
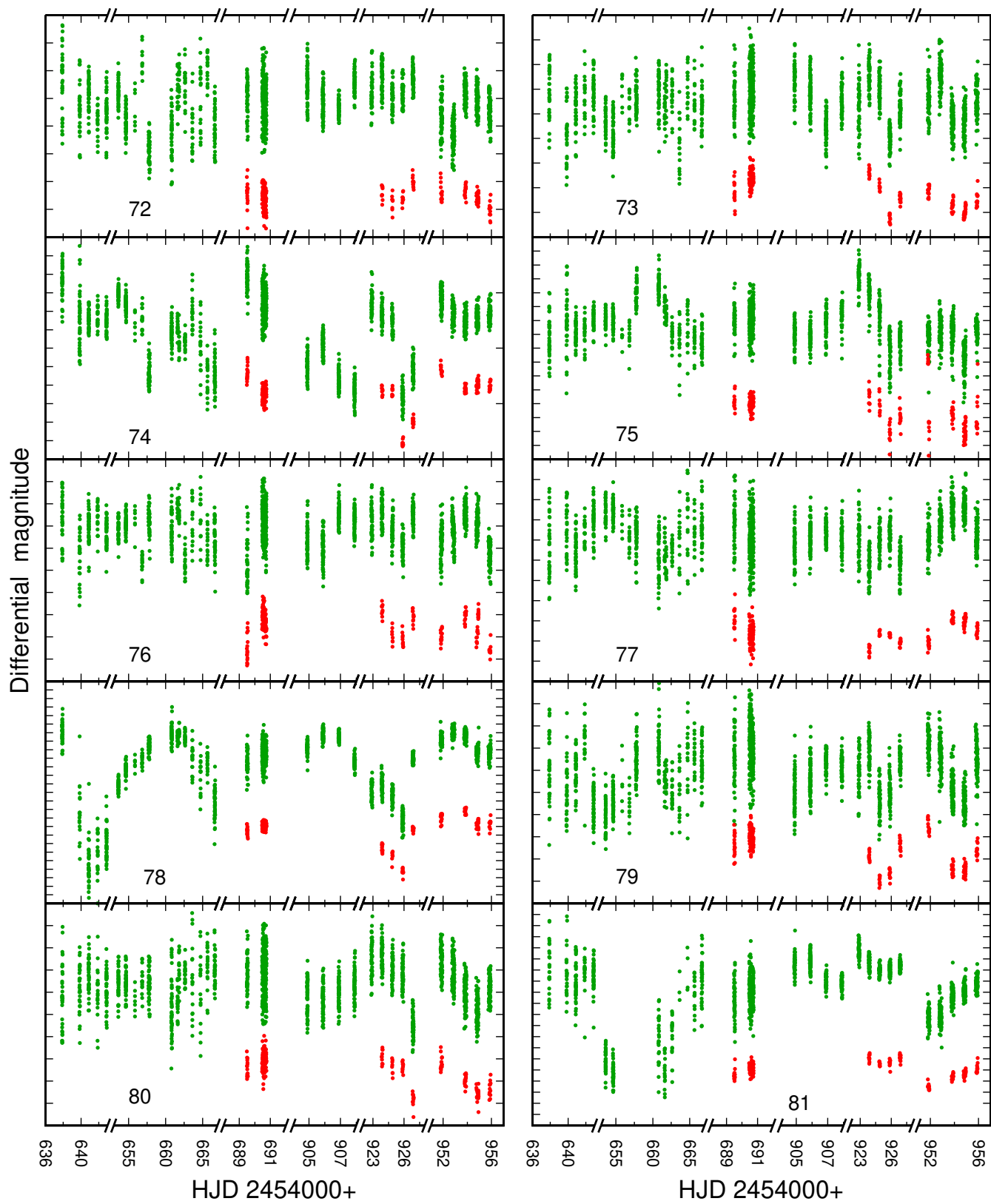


Figure B2 – *continued*

Figure B2 – *continued*

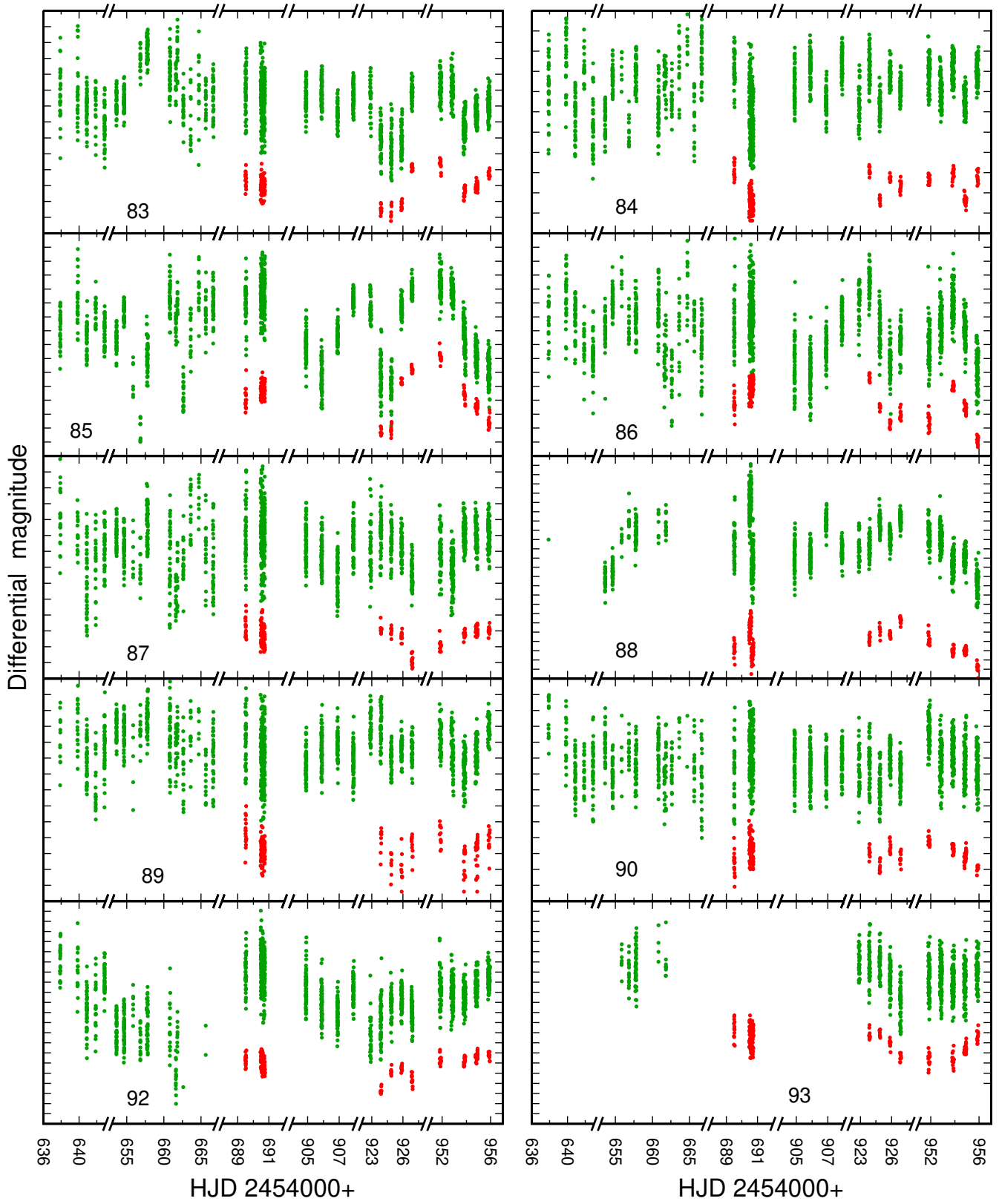


Figure B2 – *continued*

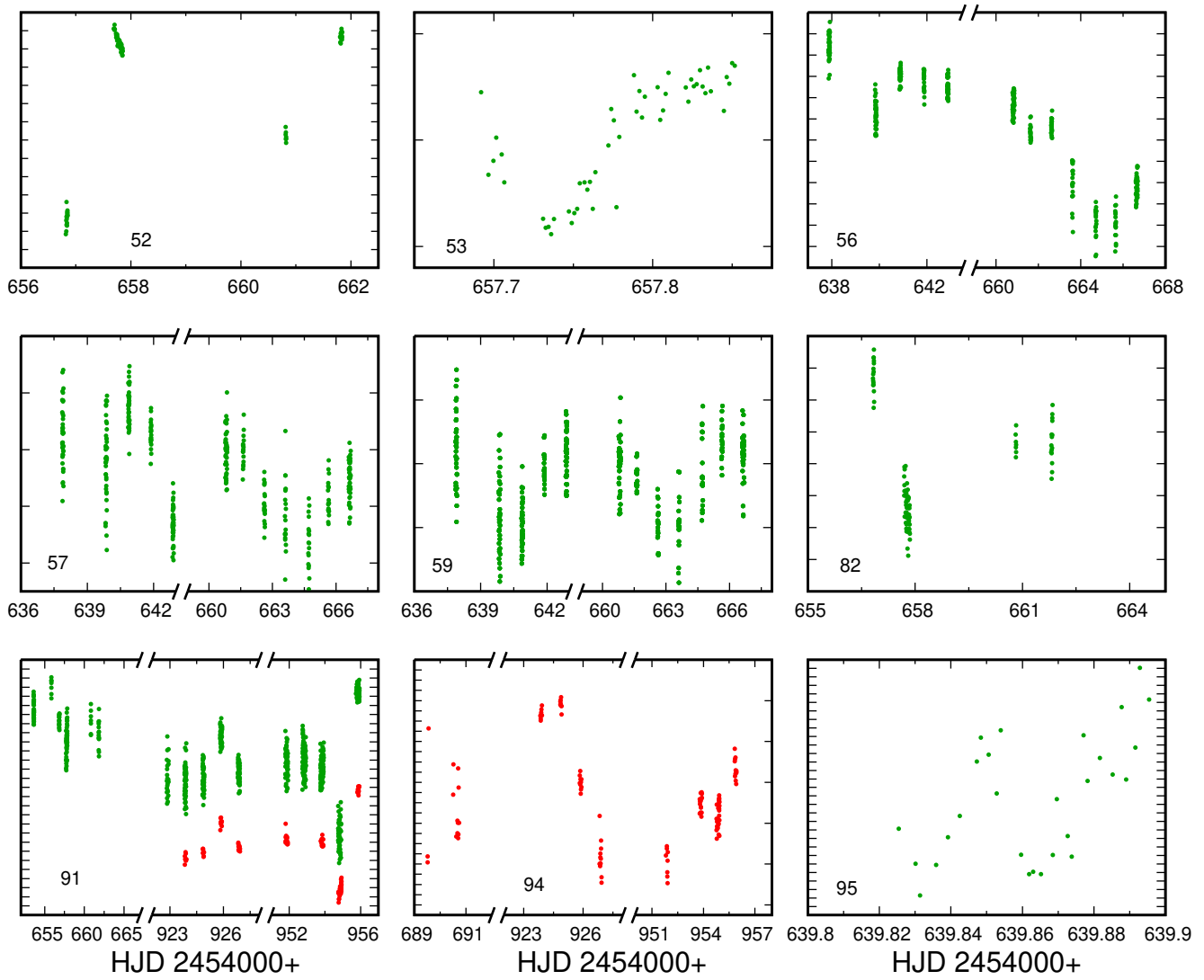


Figure B3. Light curves of V observations of irregular variables observed during only few days field of NGC6611. The ordinate ticks are separated by 0.1 mag.

ACKNOWLEDGEMENTS

This research has made use of the VizieR catalogue access tool, CDS, Strasbourg, France (DOI : 10.26093/cds/vizieR). The original description of the VizieR service was published in 2000, A&AS 143, 23.

This research has made use of the WEBDA database, operated at the Department of Theoretical Physics and Astrophysics of the Masaryk University.

This work has made use of data from the European Space Agency (ESA) mission *Gaia* (<https://www.cosmos.esa.int/gaia>), processed by the *Gaia* Data Processing and Analysis Consortium (DPAC, <https://www.cosmos.esa.int/web/gaia/dpac/consortium>). Funding for the DPAC has been provided by national institutions, in particular the institutions participating in the *Gaia* Multilateral Agreement.

This publication makes use of data products from the Two Micron All Sky Survey, which is a joint project of the University of Massachusetts and the Infrared Processing and Analysis Center/California Institute of Technology, funded by the National Aeronautics and Space Administration and the National Science Foundation.

This research has made use of the NASA/IPAC Infrared Science Archive, which is funded by the National Aeronautics and Space Administration and operated by the California Institute of Technology.

This work is based in part on observations made with the Spitzer Space Telescope, which is operated by the Jet Propulsion Laboratory, California Institute of Technology under a contract with NASA.

Based on data products from observations made with ESO Telescopes at the La Silla Paranal Observatory under public survey programme ID, 177.D-3023.

This work is based in part on data obtained as part of the UKIRT Infrared Deep Sky Survey.

The observations were supported by Chilean Fondecyt Project 3085010 realised at the Universidad de Concepción.

We are indebted to Prof. Andrzej Pigulski for his comments made upon reading the manuscript.

REFERENCES

- Ababakr K. M., Oudmaijer R. D., Vink J. S., 2017, *MNRAS*, **472**, 854
- Andre P., Ward-Thompson D., Barsony M., 1993, *ApJ*, **406**, 122
- Barentsen G., et al., 2011, *MNRAS*, **415**, 103
- Barrado y Navascués D., Martín E. L., 2003, *AJ*, **126**, 2997
- Belikov A. N., Kharchenko N. V., Piskunov A. E., Schilbach E., 1999, *A&AS*, **134**, 525
- Belikov A. N., Kharchenko N. V., Piskunov A. E., Schilbach E., 2000, *A&A*, **358**, 886
- Benjamin R. A., et al., 2003, *PASP*, **115**, 953
- Bertout C., 1989, *ARA&A*, **27**, 351
- Bertout C., Siess L., Cabrit S., 2007, *A&A*, **473**, L21
- Bessell M. S., Brett J. M., 1988, *PASP*, **100**, 1134
- Bosch G. L., Morrell N. I., Niemelä V. S., 1999, *Rev. Mex. Astron. Astrofis.*, **35**, 85
- Bouvier J., Alencar S. H. P., Harries T. J., Johns-Krull C. M., Romanova M. M., 2007, in Reipurth B., Jewitt D., Keil K., eds, *Protostars and Planets V*. p. 479 ([arXiv:astro-ph/0603498](https://arxiv.org/abs/astro-ph/0603498))
- Bressan A., Marigo P., Girardi L., Salasnich B., Dal Cero C., Rubele S., Nanni A., 2012, *MNRAS*, **427**, 127
- Caldwell J. A. R., Cousins A. W. J., Ahlers C. C., van Wamelen P., Maritz E. J., 1993, *South African Astronomical Observatory Circular*, **15**, 1
- Carpenter J. M., 2001, *AJ*, **121**, 2851
- Casali M., et al., 2007, *A&A*, **467**, 777
- Cutri R. M., et al., 2003, *VizieR Online Data Catalog*, p. II/246
- De Marchi G., Panagia N., Romaniello M., 2010, *ApJ*, **715**, 1
- Drew J. E., et al., 2005, *MNRAS*, **362**, 753
- Drew J. E., et al., 2014, *MNRAS*, **440**, 2036
- Duchêne G., Simon T., Eislöffel J., Bouvier J., 2001, *A&A*, **379**, 147
- Dutta S., Mondal S., Joshi S., Jose J., Das R., Ghosh S., 2018, *MNRAS*, **476**, 2813
- Evans C. J., et al., 2005, *A&A*, **437**, 467
- Feigelson E. D., Decampli W. M., 1981, *ApJ*, **243**, L89
- Flaherty K. M., Pipher J. L., Megeath S. T., Winston E. M., Gutermuth R. A., Muzerolle J., Allen L. E., Fazio G. G., 2007, *ApJ*, **663**, 1069
- Gaia Collaboration 2020, *VizieR Online Data Catalog*, p. I/350
- Gaia Collaboration 2022, *VizieR Online Data Catalog*, p. I/358
- Gaia Collaboration et al., 2016, *A&A*, **595**, A1
- Galli P. A. B., Bertout C., Teixeira R., Ducourant C., 2015, *A&A*, **580**, A26
- Greene T. P., Wilking B. A., Andre P., Young E. T., Lada C. J., 1994, *ApJ*, **434**, 614
- Guarcello M. G., Prisinzano L., Micela G., Damiani F., Peres G., Sciortino S., 2007, *A&A*, **462**, 245
- Guarcello M. G., Micela G., Damiani F., Peres G., Prisinzano L., Sciortino S., 2009, *A&A*, **496**, 453
- Guarcello M. G., Caramazza M., Micela G., Sciortino S., Drake J. J., Prisinzano L., 2012, *ApJ*, **753**, 117
- Gutermuth R. A., Megeath S. T., Myers P. C., Allen L. E., Pipher J. L., Fazio G. G., 2009, *ApJS*, **184**, 18
- Hawley S. L., Davenport J. R. A., Kowalski A. F., Wisniewski J. P., Hebb L., Deitrick R., Hilton E. J., 2014, *ApJ*, **797**, 121
- Heinze A. N., et al., 2018, *AJ*, **156**, 241
- Henderson C. B., Stassun K. G., 2012, *ApJ*, **747**, 51
- Herbig G. H., 1960, *ApJS*, **4**, 337
- Herbig G. H., 1977, *ApJ*, **217**, 693
- Herbig G. H., 1989, in Reipurth B., ed., *European Southern Observatory Conference and Workshop Proceedings Vol. 33, European Southern Observatory Conference and Workshop Proceedings*. pp 233–246
- Herbig G. H., Dahm S. E., 2001, *PASP*, **113**, 195
- Herbst W., Shevchenko V. S., 1999, *AJ*, **118**, 1043
- Herbst W., Herbst D. K., Grossman E. J., Weinstein D., 1994, *AJ*, **108**, 1906
- Herbst W., Bailer-Jones C. A. L., Mundt R., 2001, *ApJ*, **554**, L197
- Hernández J., Calvet N., Hartmann L., Briceno C., Sicilia-Aguilar A., Berlind P., 2005, *AJ*, **129**, 856
- Hewett P. C., Warren S. J., Leggett S. K., Hodgkin S. T., 2006, *MNRAS*, **367**, 454
- Hillenbrand L. A., Massey P., Strom S. E., Merrill K. M., 1993, *AJ*, **106**, 1906
- Hiltner W. A., Iriarte B., 1955, *ApJ*, **122**, 185
- Indebetouw R., Robitaille T. P., Whitney B. A., Churchwell E., Babler B., Meade M., Watson C., Wolfire M., 2007, *ApJ*, **666**, 321
- Jayasinghe T., et al., 2018, *MNRAS*, **477**, 3145
- Joy A. H., 1945, *ApJ*, **102**, 168
- Kalari V. M., 2019, *MNRAS*, **484**, 5102
- Kalari V. M., et al., 2015, *MNRAS*, **453**, 1026
- Kamp L. W., 1974, *A&AS*, **16**, 1
- Kenyon S. J., Hartmann L., 1987, *ApJ*, **323**, 714
- Koenigl A., 1991, *ApJ*, **370**, L39
- Kóspál Á., Ábrahám P., Zsidi G., Vida K., Szabó R., Moór A., Pál A., 2018, *ApJ*, **862**, 44

- Kuhn M. A., Hillenbrand L. A., Sills A., Feigelson E. D., Getman K. V., 2019, *ApJ*, **870**, 32
- Kumar B., Sagar R., Sanwal B. B., Bessell M. S., 2004, *MNRAS*, **353**, 991
- Lada C. J., 1987, in Peimbert M., Jugaku J., eds, IAU Symposium Vol. 115, Star Forming Regions. pp 1–17
- Lada C. J., et al., 2006, *AJ*, **131**, 1574
- Lamm M. H., Mundt R., Bailer-Jones C. A. L., Herbst W., 2005, *A&A*, **430**, 1005
- Lata S., Pandey A. K., Kesh Yadav R., Richichi A., Irawati P., Panwar N., Dhillon V. S., Marsh T. R., 2019, *AJ*, **158**, 68
- Lucas P. W., et al., 2008, *MNRAS*, **391**, 136
- Martayan C., Floquet M., Hubert A. M., Fabregat J., Frémat Y., Baade D., Neiner C., 2007, in Bouvier J., Chalabaev A., Charbonnel C., eds, SF2A-2007: Proceedings of the Annual meeting of the French Society of Astronomy and Astrophysics. p. 518 ([arXiv:0709.2823](https://arxiv.org/abs/0709.2823))
- Martayan C., Floquet M., Hubert A. M., Neiner C., Frémat Y., Baade D., Fabregat J., 2008, *A&A*, **489**, 459
- Massey P., Johnson K. E., Degioia-Eastwood K., 1995, *ApJ*, **454**, 151
- Mendigutía I., 2020, *Galaxies*, **8**, 39
- Mendigutía I., Calvet N., Montesinos B., Mora A., Muzerolle J., Eiroa C., Oudmaijer R. D., Merín B., 2011, *A&A*, **535**, A99
- Meyer M. R., Calvet N., Hillenbrand L. A., 1997, *AJ*, **114**, 288
- Michalska G., 2019, *MNRAS*, **487**, 3505
- Munari U., Carraro G., 1996, *A&A*, **314**, 108
- Muzerolle J., Calvet N., Hartmann L., 1998, *ApJ*, **492**, 743
- Neubauer F. J., 1943, *ApJ*, **97**, 300
- Oliveira J. M., Jeffries R. D., van Loon J. T., Littlefair S. P., Naylor T., 2005, *MNRAS*, **358**, L21
- Pecaut M. J., Mamajek E. E., 2013, *ApJS*, **208**, 9
- Petrov P. P., 2003, *Astrophysics*, **46**, 506
- Rieke G. H., Lebofsky M. J., 1985, *ApJ*, **288**, 618
- Rodríguez E., Breger M., 2001, *A&A*, **366**, 178
- Romanova M. M., Ustyugova G. V., Koldoba A. V., Lovelace R. V. E., 2012, *MNRAS*, **421**, 63
- Samus' N. N., Kazarovets E. V., Durlevich O. V., Kireeva N. N., Pastukhova E. N., 2017, *Astronomy Reports*, **61**, 80
- Sana H., Gosset E., Evans C. J., 2009, *MNRAS*, **400**, 1479
- Sanders W. L., 1971, *A&A*, **14**, 226
- Sariya D. P., Yadav R. K. S., Bellini A., 2012, *A&A*, **543**, A87
- Shu F., Najita J., Ostriker E., Wilkin F., Ruden S., Lizano S., 1994, *ApJ*, **429**, 781
- Shultz M. E., Alecian E., Petit V., Bagnulo S., Böhm T., Folsom C. P., Wade G. A., MiMeS Collaboration 2021, *MNRAS*, **504**, 3203
- Spitzer Science C., 2009, VizieR Online Data Catalog, [p. II/293](https://vizier.cfa.harvard.edu/votable/?outfmt=table&source=spitzer)
- Stetson P. B., 1987, *PASP*, **99**, 191
- Stoop M., Kaper L., de Koter A., Guo D., Lamers H. J. G. L. M., Rieder S., 2022, arXiv e-prints, [p. arXiv:2207.08452](https://arxiv.org/abs/2207.08452)
- Sugitani K., et al., 2002, *ApJ*, **565**, L25
- The P. S., de Winter D., Perez M. R., 1994, *A&AS*, **104**, 315
- Tucholke H. J., Geffert M., The P. S., 1986, *A&AS*, **66**, 311
- Uribe A., Brieva E., 1994, *Ap&SS*, **214**, 171
- Vasilevskis S., Klemola A., Preston G., 1958, *AJ*, **63**, 387
- Vink J. S., Drew J. E., Harries T. J., Oudmaijer R. D., 2002, *MNRAS*, **337**, 356
- Walker M. F., 1961, *ApJ*, **133**, 438
- Walter F. M., 1986, *ApJ*, **306**, 573
- Walter F. M., Kuhl L. V., 1981, *ApJ*, **250**, 254
- Walter F. M., Brown A., Mathieu R. D., Myers P. C., Vrba F. J., 1988, *AJ*, **96**, 297
- Watson C. L., Henden A. A., Price A., 2006, Society for Astronomical Sciences Annual Symposium, **25**, 47
- Wolff S. C., Strom S. E., Dror D., Venn K., 2007, *AJ*, **133**, 1092
- Zhao J. L., He Y. P., 1990, *A&A*, **237**, 54
- Zwintz K., 2008, *ApJ*, **673**, 1088
- de Winter D., Koulis C., The P. S., van den Ancker M. E., Perez M. R., Bibo E. A., 1997, *A&AS*, **121**, 223

This paper has been typeset from a $\text{\TeX}/\text{\LaTeX}$ file prepared by the author.